Ph.D. Thesis

Runx1/Cbfb-Stat3-Tgfb3 signaling network modulates anterior region palatogenesis

Safiye Esra Sarper

Department of Orthodontics and Dentofacial Orthopedics

Course for Molecular Oral Biology and Dentistry

Osaka University Graduate School of Dentistry,

Osaka, Japan

2018

ABSTRACT

The cleft lip and/or palate (CLP) is one of the congenital birth defects which has complex etiology. In order to accomplish the palatogenesis, precise temporospatial cellular and molecular regulation are essential and failure of either step could result in cleft palate. The mechanism of posterior palatogenesis is relatively well studied, however, the mechanism of anterior palatogenesis is largely elusive. Past study reported that *Runx1* loss mouse exhibited an anterior cleft palate. Runx1 is one of Runx gene family which work redundant and cooperative in several tissues. Cbfb is cofactor enhances their DNA-binding capacity and required for Runx dependent transcriptional regulation. To reveal *Runx1* related cleft etiology and possible redundancy between Runx genes, we used *Runx1* deficient mouse and *Cbfb* deficient mouse. In this study, both of epithelial-specific *Runx1* and *Cbfb* knock out mice demonstrated an anterior cleft with the persistent epithelial layer that disturbs the epithelial disintegration with mesenchymal confluence. Runx1/Cbfb deficiency resulted in anterior region specific downregulation of *Tgfb3* claimed Runx1/Cbfb-Tgfb3 pathway is region specific. The similarity between *Runx1* and *Cbfb* loss mouse phenotypes indicated that *Runx1* is the major gene in Runx1/Cbfb signaling regulating anterior palatogenesis. Furthermore, Stat3 phosphorylation was substantially disturbed at cleft regions in Runx1/Cbfb mutants. Pharmacological treatment of Stat3 inhibitor on wild-type palates demonstrated an anterior cleft with marked downregulation of *Tgfb3*. Altogether in this study, we identified Runx1/Cbfb-Jak/Stat-Tgfb3 as anterior palate specific novel gene network that is critical for anterior palate fusion via regulating apoptosis and proliferation functions in fusing epithelium.

INTRODUCTION

Craniofacial development requires the coordinated accumulation of signals from the endoderm, mesoderm, ectoderm, neuroectoderm and neural crest cells. On the grounds of this complexity, craniofacial deficiencies are causes of several birth defects and lethality in the embryonic stage. The facial processes do not express the classical *Hox* genes which in other regions of the body determine patterning. Several growth factors, such as *Shh, Fgf8, Tgfb*, and *Bmp4* or retinoic acid signaling control the growth and patterning of the face through epithelial-mesenchymal signaling interactions [1].

Development of head in mammals starts with five facial prominences formation. These prominences are the frontonasal prominence at the rostral side, two maxillary prominences at two lateral side and two mandibular prominences at caudal side. The frontonasal prominence is divided two parts by the formation of nasal pits. As development proceeds, these two parts; medial and lateral nasal processes and the maxillary prominences form the palate tissue, respectively [2].

Two maxillary prominences form the posterior part of the palate [3]. Anterior part of palate is formed by the medial nasal process and two maxillary prominences [2]. The posterior part of the palate as known as the secondary palate formation incorporates outgrowth, which initially grows vertically and subsequently reorients to grow horizontally above the dorsum of the tongue in a palatal shelf elevation process. After continued horizontal growth two palatal shelves meet at midline. Following the contact of palatal shelves, the fusion occurs with formation of the epithelial seam which disintegrates later to ensure mesenchymal continuity. This complex fusion

process begins from secondary palate middle region continues through anterior and posterior directions. Furthermore, anterior edge of secondary palate fuses with the primary palate and an anterodorsal edge of secondary palate fuses with nasal septum simultaneously [4]. During fusion process, the epithelium between the secondary palatal shelves, named as midline epithelial seam (MES) must be disintegrated to ensure mesenchymal continuity. Recent studies have disclosed the mechanisms of fusing epithelium disintegration with some aspects remaining controversial [5]. Cell death is proposed mechanism for epithelium disintegration from several studies that show TUNEL positive and caspase3 positive cells in MES [6-8]. In addition to this, excessive proliferation activity at fusing epithelium leads to the persistent epithelium and further resulted in fusion failure [9]. Moreover, there is periderm layer which is formed by flattened epithelial layer on fusing epithelial seam. Periderm acts as a barrier to prevent premature adhesions during embryogenesis [10]. Formation and removal of periderm determine the palate fusion fate [11]. In mice palatogenesis, palate processes first detectable by embryonic day 11.5 and complete by E17 after fusion of palate processes. Disruption of any of these processes in this interval can be concluded with cleft palate. Cleft lip and palate (CLP) is the very frequent congenital birth defect which can be classified as syndromic and non-syndromic based on the existence of additional birth defects [12, 13]. Syndromic CLP etiology incorporates chromosomal aberrations. On the other hand, non-syndromic CLP etiology is related with the complex interaction between genetic and environmental factors [13].

Palatogenesis is regulated by an extensive and several molecular pathways. Some of them; *Shh, Tgfb3, Shox2, Msx1, Bmp4, Pax9* and *Fgf10* have been intensely investigated [14-17]. These investigations implicated that several genes demonstrated

different expression patterns in region-specific manner [4]. Such heterogeneity of expressions seems to be related to the regional difference at palate formation. Based upon complex development process there are many studies using mouse models that have a cleft phenotype. Conditional inactivation of *Shh* in the epithelium leads to a cleft palate phenotype, suggesting the critical role of *Shh* in palate development [18]. Conversely, the *Shh*-expressing transgenic mouse had demonstrated a complete cleft resulted from lack of apoptosis in fusing epithelium [14]. *Tgfb3* null mouse exhibited cleft due to the requirement of *Tgfb3* for fusion of palatal shelves through leading MES to disintegration via periderm layer removal, apoptosis regulation [19-21]. Strikingly, TGFβ3 exogenous addition in an *in vitro* culture system could rescue the *Tgfb3* null mouse cleft [20, 21]. In human, reports showed TGFβ3 gene variants associated with increased risk of non-syndromic CLP [22-24]. These studies predominantly investigated the etiology lies under secondary palate cleft which is placed at the posterior region. Conversely, there are not many anterior region cleft mouse model which might the reason of inadequate information about anterior palate fusion mechanism. Few mouse models have been investigated as anterior palatogenesis related genes. The *Msx1*-BMP4 transgenic mouse has demonstrated anterior cleft [25]. *Shox2*$^{-/-}$ mice developed a rare type of cleft that is restrained to the anterior palate region [16]. We previously reported the same type of cleft limited at anterior area using *Runx1* conditionally rescued mouse [26].

Runx1 is a member of *Runx* family genes which work as transcription factors [27]. *Runx* family genes play crucial roles at embryogenesis with *Runx1* being need of hematopoiesis, *Runx2* being need of osteogenesis, *Runx3* being need of neurogenesis. Strikingly, recent studies have spotted on their roles at the adult stage such as cancer formation by regulating critical cellular mechanisms [28-30]. *Runx* family

genes make a heterodimer complex with Core binding factor beta (Cbfb) which is a co-transcription factor enhancing their DNA-binding capacity [31]. *Cbfb* is required for *Runx* related transcriptional regulation. There is only one β subunit which is *Cbfb* while the α subunit is encoded by three genes: *Runx1, Runx2*, and *Runx3*. *Runx* genes all require *Cbfb* for their function [32]. Due to this relation, several studies have shown the phenotypic similarity between *Cbfb* mutants and *Runx* genes mutants. Since *Runx* family genes expression patterns overlap in several tissues, functional redundancy and cooperation between *Runxs* have been studied intensively [33-35].

Previous studies have shown Runx/Cbfb signaling genes cooperative functions and significant roles in morphogenesis of various tissues [36, 37]. During lacrimal gland (LG) morphogenesis *Runx* factors are needed for their roles in growth and branching. LG treated with combined *Runx1, Runx2,* and *Runx3* siRNAs showed greatly reduced branching and irregular bud shape. Thus, *Runx1, Runx2,* and *Runx3* are partially redundant in LG morphogenesis [38]. Epithelial *Cbfb* loss leads to the decrease in the size of the submandibular gland (SMG) and in the saliva secretion [39]. Moreover, *Runx1* mutant mouse demonstrated similar submandibular gland phenotype [37]. *Runx2* deficiency resulted in the misshapen and severely hypoplastic tooth. During tooth formation, *Runx2* regulates the molecule expressions to control growth and differentiation [40]. Other than involvement in morphogenesis stage, Runx/Cbfb signaling involvement in stem cells has been implied in the incisor stem cells. *Cbfb* modulates ameloblast differentiation and maintenance of stem cells during tooth formation [36]. Hair follicle (HF) development is another topic of *Runx* genes stem cell involvement. *Runx2* null mice exhibit a significant delay in HF development and a noticeable decrease in epidermal and overall skin thickness [41]. *Runx1* epithelial loss leads to impaired HF morphogenesis. *Runx1* role at HF development incorporates

regulation of the epithelial-mesenchymal crosstalk, differentiation, and proliferation [42]. Both of morphogenesis and stem cell studies claimed Runx/Cbfb signaling regulation of various signaling molecules and critical cellular functions. About palate morphogenesis, the previous study used *Runx1* conditionally rescued mouse demonstrated anterior specific cleft [26]. However, detailed cellular mechanism and molecular mechanism of *Runx1* related cleft pathogenesis were not identified.

In human, RUNX1 mutations were reported with acute myeloid leukemia [43]. RUNX1 microdeletion involved Braddock-Carey syndrome patients reported with congenital thrombocytopenia, broad nasal root, thick everted vermilion of the lower lip with an inverted U-shaped vermilion of the upper lip, and lack of facial expression with enamel hypoplasia and cleft palate [44]. CBFB gene is localized to 16q22.1 in human [45]. The case report of a patient with a 16q22 deletion presented a large fontanelle of the skull, midface hypoplasia, prominent earlobes, short columella, medial eyebrow flare, broad nasal tip, bifid uvula and cleft palate [46]. Moreover CBFB haploinsufficiency in human reported with delayed cranial ossification, congenital heart anomalies, hypertelorism, midface hypoplasia, micrognathia, delayed skull ossification and cleft palate [47]. Despite many reports claimed Runx/Cbfb signaling involvement in palatogenesis, roles of *Runx1* or Runx/Cbfb signaling during palate formation and either redundancy or cooperativity existence between *Runx* genes was not elucidated yet.

The Janus kinase-signal transducer and activator of transcription (JAK-STAT) signaling pathway is activated in response to cytokines, hormones and growth factors [48]. This large cascade transduces multitude signals during development by regulating critical cellular mechanisms; cell proliferation, differentiation, cell migration, and apoptosis. In mammals, there are four members of JAK family; JAK1

(Jakus Kinase 1), JAK2, JAK3, and Tyk2 (Tyrosine kinase). JAK activation is required for phosphorylation of STATs (Signal transducer and activator of transcription). STATs are latent transcription factors placed in the cytoplasm until activated. Subsequently activated JAKs phosphorylate STATs. Phosphorylated STATs enter the nucleus and then they bind to specific regulatory sequences in order to activate or repress target genes. Recent studies have shown STATs role in development and homeostasis of several tissues [49-51]. Among the Stat proteins, STAT3 plays most diverse and crucial roles in a variety of physiological functions including growth, anti-apoptosis, apoptosis and cell motility conditional upon the cell type and stimulus [52, 53]. Physiological functions of Stat3 has been intensely investigated in both of cancer formation and hair cycle processes [49, 54]. During epithelial cancer formation, Runx1-Stat3 activation is needed for regulating proliferation and cancer growth [55]. Runx1-Stat3 axis also implied in hair cycle regulation [42]. However, there is no study about Runx1-Stat3 regulation at palatogenesis.

To address these issues we used two different mice carrying conditional knock out of *Runx1* and *Cbfb* genetic background. These two mice exhibit anterior specific clefting between primary and secondary palate. Before the fusion between primary and secondary palates, size similarity of palate processes between control and Runx1/Cbfb signaling deficient mice claimed fusion process as etiology of the cleft. Fusion region epithelium of Runx1/Cbfb signaling loss mouse demonstrated persistent proliferation with decreased cell death. Moreover, Runx1/Cbfb signaling loss related anterior region-specific *Tgfb3* expression downregulation and decreased Stat3 activation were found as responsible molecular deviations of anterior cleft pathogenesis.

MATERIALS AND METHODS

1. Animals

Runx1$^{-/-}$ mice are lethal due to hemorrhage at about E12.5 when the palatal development is not yet initiated [26]. To find out the role of Runx1 in oral epithelium, we use epithelial specific knock out mouse created through Cre/*loxP* system (K14-Cre/*Runx1*$^{fl/fl}$). C57BL/6J mice picked as the genetic background in this study. Besides this, to uncover other *Runx* genes role at palate formation we used epithelial specific *Cbfb* knock out mouse(K14-Cre/*Cbfb*$^{fl/fl}$). *Cbfb* homozygous null mutant embryos exhibit hemorrhaging at central nervous system, impaired definitive hematopoiesis, and lethal around E12.5 [56].

To generate K14-Cre/*Runx1*$^{fl/fl}$ mice, we first mated heterozygous K14-Cre mice and *Runx1*$^{fl/fl}$ mice to obtain *K14-Cre/Runx1*$^{fl/+}$ mice. These progenies were subsequently bred with *Runx1*$^{fl/fl}$ mice. K14-Cre/*Cbfb*$^{fl/fl}$ mouse was also generated with the same way. Genomic DNA was isolated from each tail sample using 50 µM NaOH, Tris HCl. Genotyping was performed by the conventional polymerase chain reaction (PCR) method using each primer set to detect *Cre* (5' CTCTGGTGTAGCTGATGATC 3' and 5' TAATCGCCATCTTCCAGCAG 3') and the *loxP* site of *Runx1* (5' GCGTTCCAAGTCAGTTGTAAGCC 3' and 5' CTGCATTTGTCCCTTGGTTGACG 3') and loxP site of *Cbfb* (5' CCTCCTCATTCTAACAGGAATC 3' and 5' GGTTAGGAGTCATTGTGATCAC 3'). We used their littermates that did not carry the K14-Cre/*Runx1*$^{fl/fl}$or K14-Cre/*Cbfb*$^{fl/fl}$ genotype as a control.

2. Laser Microdissection

The mice embryonic maxillas were freshly embedded in OCT compound and frozen immediately. Tissues are serially sectioned at −20°C on a cryostat (CM 1950, Leica) at a thickness of 25μm. The maxilla was sectioned from anterior to posterior throughout anterior palate until the secondary palate appeared. The tissue sections were mounted and thawed on a film-coated slide. In total, there were 12-14 serial sections obtained from the anterior palate at E15.0 (section numbers varied due to the orientation of the frozen block). We stained these slides with cresyl violet dye staining. Anterior palate epithelial and mesenchymal tissue was dissected from the sections using a Leica Micro Laser System (LMD6500, Leica) and collected by tube.

3. RNA Extraction and Real-Time RT-PCR Analysis

We used the laser microdissected tissues of the control and K14-Cre*/Runx1*$^{fl/fl}$ mice for extracting total RNA. IsogenII (Nippon Gene, Toyama, Japan) is used to extract total RNA and performed according to the manufacturer's protocol. Total RNA was reverse transcribed to cDNA using an oligo (dT) with avian myeloblastosis virus reverse transcriptase (Takara, Osaka, Japan). For the Real-time RT-PCR analysis, the cDNA was amplified with Taq DNA Polymerase (Toyobo Sybr Green Plus, Osaka, Japan) using a light cycler (Roche). The thermal profile for all SYBR Green PCRs was 95°C for 30s followed by 50 cycles of 3 step amplification including 95°C for 5s, 55°C for 10s, 72°C for 15s and melting step including 95°C for 1s, 73°C for 15s, 95°C for 1s 60°C and 40°C 30s for cooling. *Gapdh* used as the housekeeping gene to normalize RNA level. Primer sequences are available in the Fig.17. At least three embryos of each genotype were used for each analysis.

4. Whole-Mount *in situ* Hybridization Analysis

Whole-mount *in situ* hybridization was performed using fixed E14.0, E14.5 and E15.0 palates. The digoxigenin-labeled RNA probes used in this study were prepared using a DIG RNA labeling kit (Roche) according to the manufacturer's protocol using each cDNA clone as the template. The probes were synthesized from fragments of Runx1, Tgfb3, Socs3, and Stat3 (Allen Institute for Brain Science) and were amplified with T7 and SP6 adaptor primers through PCR. After hybridization, the expression patterns for each mRNA were detected and visualized according to their immunoreactivity with anti-digoxigenin alkaline phosphatase-conjugated Fab fragments (Roche), as previously reported. Probes for Shh[14], Bmp4, Shox2[16], Msx1 generated through using some of the constructs from our plasmid stock. At least three embryos of each genotype were used for each analysis.

5. TUNEL staining

Apoptotic cells were identified by TUNEL (terminal deoxynucleotidyl transferase-mediated dUTP nick end labeling) and the standard protocol for frozen sections was followed (ApopTag, Chemicon). Frozen sections (10 μm) from samples were prepared, fixed in 1% PFA in PBS for 10 min at room temperature, rinsed in PBS, postfixed in ethanol/acetic acid (2:1) for 5 min at − 20°C, and then incubated in 3% H_2O_2 for 5 min to quench endogenous peroxidases.

6. 5-Bromo-3-deoxy-uridine labeling

5-Bromo-3-deoxy-uridine (BrdU) (Invitrogen) was injected intraperitoneally at 10 µl/g body weight of pregnant mouse at prenatal day 15, 2 hours before their sacrifice. After the mice had been sacrificed, we take out palate using fine scissors, fixed them overnight at 4°C in 4% paraformaldehyde in PBS. Frozen sections (10µm) from samples were prepared. Trypsin was applied for 10 min at 37 °C and the standard protocol for frozen sections was followed (BrdU Staining Kit, Invitrogen). The sections were counterstained with hematoxylin.

7. Assessment of palatal fusion and a histological analysis

The mouse embryonic heads were dissected in BGJb medium (Gibco). The palate was evaluated by direct observation and with a dissecting microscope. These tissues were fixed in 4% paraformaldehyde, equilibrated in graded sucrose, and embedded in Tissue-Tek (OCT compound, Sakura). Frozen sections (20µm) from samples were prepared. For histological analysis, we applied hematoxylin-eosin staining.

8. Immunohistochemistry

Immunofluorescence staining was performed on 20-µm sections using polyclonal rabbit-anti-Ki67 (1:400, ab15580, Abcam), monoclonal rabbit anti-K17 (1:200, #4543, Cell Signaling Technology), polyclonal rabbit anti-K6A (1:200, 905701, Biolegend), monoclonal anti-K14 (1:200, ab7880, Abcam), monoclonal rabbit anti-phospho-Stat3 (pStat3, 1:200, #9145, Cell Signaling Technology), and monoclonal rabbit anti-Stat3 (1:200, #9139, Cell Signaling Technology) overnight at 4°C. Then, Alexa488-

conjugated goat-anti-rabbit IgG (1:400, A21206, Molecular Probes) or Alexa546-conjugated goat-anti-mouse IgG (1:400, A11003, Molecular Probes) was used as secondary antibody for 3 h at room temperature. The sections were then counterstained with DAPI (1:500, Dojindo) and mounted with fluorescent mounting medium (Dako). At least three embryos of each genotype were used for each analysis.

9. *in vitro* culture of palatal shelves and rescue of the mutant cleft palate

The palate was dissected from the E15.0 embryo and cultured on track-etched polycarbonate membrane filter (Nuclepore) in Trowell type organ culture with serumless, chemically defined BGJb medium (Gibco). Affi-Gel beads (Bio-Rad) were incubated in TGFB3 (100 ng/μl, R&D Systems). Bovine serum albumin (BSA; Sigma-Aldrich) was used instead of recombinant protein for the control beads. The beads were immersed in recombinant protein or BSA at 37 °C for 60 min and placed on the primary palate of the explants using a pipette tube. After culture, the *in vitro* explants were fixed at each stage in 4% paraformaldehyde overnight and then processed for histological examination and qPCR analyses.

10. Whole-head roller culture assays and treatment of Stat3 inhibitor

Embryo heads from E13.0, E14.0 ICR mouse embryos were collected in BGJB and mandibles, tongues, and brains were removed. The remaining palatal tissues including the primary, the secondary palate, and the nasal septum were cultured for 24-48 h in whole-embryo culture incubator (RKI Ikemoto) at 37 °C (Iseki, Osumi).

Palatal tissues were incubated in BGJb medium with or without AG490 (200-400 μM; Sigma-Aldrich) or STAT3 Inhibitor VI, S3I-201 (200-400 μM; Sigma-Aldrich). Tissues were harvested after 24 h of culture and fixed in 4% paraformaldehyde for processing, or samples were processed with qPCR.

11. Western Blot Analysis

The dissected palatal tissues were lysed with RIPA buffer (nacalai tesque) supplemented with protease and phosphatase inhibitors (nacalai tesque). The lysates were centrifuged and the supernates were heated in denaturing Laemmli buffer (Bio-rad Laboratories). Proteins were separated by SDS-PAGE and transferred to Polyvinylidene difluoride membranes (Biorad Laboratories). The membranes were incubated with either anti-Stat3 (1:1000, #9139, Cell Signaling Technology), anti-pStat3 (1:1000, #9145, Cell Signaling Technology) or beta-actin (1:2000, Sigma). The bound antibodies were detected with the HRP-linked antibody (1:1,000, Cell Signaling Technology) and the ECL detection kit (Bio-rad Laboratories).

12. X-Gal Staining

The Cre reporter strain (B6.129S4-*Gt(ROSA)26*^{Sortm1Sor}*/J*; R26R was used to confirm K14-Cre efficiency [57]. We mated K14-Cre and R26R conditional reporter allele R26R mice [58] to generate K14-Cre; R26R mice. Mice maxillas were dissected at E15.0 and fixed in 0.2% glutaraldehyde and 2% formaldehyde in PBS containing 2 mM $MgCl^2$, and embedded in Tissue-Tek (OCT compound, Sakura, Tokyo, Japan).

The samples were then sectioned into 20 μm sections and incubated in 5-Bromo-4-chloro-3-indoxyl-b-D-galactopyranoside(X-Gal) solution at 37°C for 12–16 hours [57].

13. Statistical analyses

Quantitative variables in two groups were compared using the Mann-Whitney U test. Differences among the three groups were determined using the analysis of variance (ANOVA) test, and significant effects indicated by the ANOVA were further analyzed with post hoc Bonferroni correction. P values < 0.05 were considered significant. Significance was determined using the statistical analysis software program JMP, version 5 (SAS Institute Inc.).

14. Study approval

Mice were housed in the animal facility at the Department of Dentistry, Osaka University. Welfare guidelines and procedures were performed with the approval of the Osaka University Graduate School of Dentistry Animal Committee.

RESULTS

1. Runx1/Cbfb signaling loss in epithelium resulted in anterior clefting

The previous study about *Runx1* conditionally rescued null mouse demonstrated limited anterior cleft at the first rugae area between the primary and the secondary palates [26]. We have previously shown *Runx1* expression in the fusing epithelium at the tip of the growing secondary palatal process [59]. In the anterior regions, the *Runx1* mRNA expression was also localized in the fusing epithelium between the primary and the secondary palates [26]. *Runx1* conditionally rescued null mouse which was analyzed in the previous study was lethal at birth, so the question was remained unanswered whether the reason of cleft is the delay in the process of growth. In order to analyze further and from the existence of intense expression of *Runx1* in epithelium we used *Runx1* epithelial conditional knock out mouse using Cre recombination. We confirmed the efficiency of the K14-Cre recombination using Rosa26R reporter mice and X-gal staining [57] in E15.0 mouse at the primary palate and secondary palate areas. X-gal staining was evident in epithelium areas and fusing epithelium, intensely (Fig. 1A). In the present study, it turned out that epithelial specific *Runx1* mutant mouse survived until adult stages and also showed anterior limited cleft (Fig. 1B) at P0 as similar to past report. At control mouse primary palates and secondary palates completely fused (Fig. 1B), leaving two small holes which anatomically known as orifices of incisive canal. Since *Runx1* loss in epithelium genetic backgrounded mouse did not lethal at development stage we further analyze cleft at other stages. Morphological analysis of later stages showed that there is

anterior cleft remained at P50 *Runx1* loss mouse (Fig. 1B) indicating that delayed process of palatal development is not the etiology of the cleft.

In this study, we evaluated *Runx1* expression via using the whole tissue to find out expression patterning through anterior to posterior. At E14.0 stage before the secondary palate fusion, *Runx1* mRNA expression located at secondary palate tips, rugaes, incisors and primary palate-nasal septum areas (Fig. 2A). After secondary palate fusion at E15.0 stage, *Runx1* mRNA expression becomes intense at fusion region of secondary palates and primary palate with considerably high expression at secondary palate fusion region (Fig. 2A). This broad *Runx1* expression patterning did not correlate to *Runx1* loss mouse phenotype. Past studies showed tissue-specific and overlapping expression patterns indicate both exclusive and redundant roles for the three *Runx* genes [60]. At lacrimal gland, *Runx1, Runx2*, and *Runx3* expressions were found at the development stage and established functional redundancy between each other [38]. In order to reveal possible compensation or functional redundancy between *Runx* genes, we demonstrated expression patterns of other *Runx* genes and *Cbfb*. *Runx2* mRNA expression at E14.0 and E15.0 also have a broad expression that contains incisors, rugaes, primary palate and secondary palate (Fig. 2A). *Runx3* mRNA expression pattern was similar to *Runx2* expression pattern (Fig. 2A). We also analyzed *Cbfb* which is the cofactor of *Runx* family genes. *Cbfb* mRNA expression at E14.0 shows such broad expression at palate (Fig. 2A). At fusion stage E15.0, *Cbfb* mRNA expression becomes intense at fusion regions of both primary and secondary palates (Fig. 2A). From these expression patterns, we hypothesized that compensation between *Runx* genes rescued the secondary palate cleft at *Runx1* loss mouse. Since the loss of *Cbfb* comprises all *Runx* transcriptional activity, we picked up *Cbfb* loss mouse as a model

to discreet the possible redundancy between *Runx* genes at palatogenesis. Epithelium-specific *Cbfb* knock out mouse also demonstrated an anterior cleft that is similar to *Runx1* loss mouse (Fig. 1B). *Cbfb* deficient mouse also survived till adult stage and demonstrated an anterior cleft (Fig. 1B). The cleft phenotype frequency in K14-Cre/*Runx1*$^{fl/fl}$ genotype confirmed mouse is 92% and the one in K14-Cre/*Cbfb*$^{fl/fl}$ mouse is 100% (Fig. 1C). As result, Runx1/Cbfb signaling disturbance in the epithelium has resulted with anterior clefting that remained till the late adult stages. This data indicated that there were no compensation or redundancy mechanisms between *Runx* genes during palate fusion process.

2. Runx1/Cbfb signaling related cleft pathogenesis etiology

Palatogenesis includes palate processes growth that followed with fusion. We first investigated the possible growth defect as cleft etiology. There is no significant difference in primary palate size between of control and *Runx1* mutant mouse before the fusion of primary palate and secondary palate processes at E15.0 (Fig. 3A). BrdU assay also showed no significant difference of proliferative cells between control and K14-Cre/*Runx1*$^{fl/fl}$ mouse that reaffirmed the nonexistence of growth defect (Fig. 3C). Thus, Runx1/Cbfb signaling deficient mouse palate processes proper growth making fusion process as etiology of the cleft.

During palate formation, the secondary palate processes fuse anteriorly with the primary palate and anterodorsally with the nasal septum. Both of primary palate and nasal septum are derived from the medial nasal process [4]. Histological analysis was done at E17.0. At control mouse fusion between primary and secondary palate was confirmed at this stage (Fig. 4A). In comparison, at the mutant mouse, the cleft

between primary and secondary palate was confirmed (Fig. 4A). More posterior sections showed a gap between nasal septum and secondary palate at the mutant mouse which is completely fused at control mouse (Fig. 4A).

Fusion between primary palate and secondary palate at proper palatogenesis is ensured by removal of the intervening epithelium which provides the mesenchymal continuity [5]. In order to visualize the intervening epithelium we immunostained Keratin 14(K14); epithelium cell marker at E15.0 fusion area. Immunohistochemistry analysis uncovered that there is disappeared epithelium areas between primary and secondary palate at control mouse (Fig. 4B). In contrast, there is K14 positive persistent epithelium entirely surround the mesenchyme at Runx1/Cbfb mutant mouse fusion area (Fig. 4B).

To reveal the character of K14 positive persistent epithelium in *Runx1* mutants we did apoptosis and proliferation analysis. Apoptosis is one of the fusion area epithelium dissolution mechanism [6-8, 61]. TUNEL analysis was done to reveal if there is apoptosis deviation. We detected some TUNEL positive cells at fusion area between primary and secondary palate at control mouse (Fig. 5A). Few TUNEL positive cells were also detected in the Runx1/Cbfb mutant mouse as well. However, the number of TUNEL positive cells critically decreased at Runx1/Cbfb loss mouse (Fig. 5A). Apoptosis analysis was also done at fused secondary palate area (Fig. 5A). There is no significant change of TUNEL positive cells in these areas which are parallel with our findings at secondary palate proper fusion in the mutant (Fig. 5A). It has also been proposed that continuous epithelium proliferation is one of cleft etiology [11]. In order to analyze proliferation in the fusion epithelium, we double-stained Ki67 as proliferative cell marker, K14 as epithelium cell marker and counterstained with DAPI. Immunoreactivity analysis demonstrated that there are

some proliferative cells being conspicuous in fusing epithelium of Runx1/Cbfb loss mouse (Fig. 6A). The number of proliferative cells is significantly increased in Runx1/Cbfb loss mouse epithelium between primary and secondary palate (Fig. 6A).

The palatal fusion epithelium is composed of a basal columnar cell layer surrounded by flat cells that form the periderm [6]. During palate fusion, periderm removal is necessary for fusing epithelium dissolution. Periderm removal deficiency was confirmed at posterior cleft exhibited mouse secondary palate fusing epithelium [11]. Conversely, there is no information about periderm existence at primary palate area. To reveal periderm layer at fusion area, K17 (Keratin 17) was used as periderm marker [10]. At control mouse K17 positive periderm layer was detected at fusion areas. There are some regions K17 immunostaining were not detected which was presumably removed with fusion (Fig. 7A). Conversely, periderm tissue had maintained between primary and secondary palate at *Runx1* loss mouse (Fig. 7A). To investigate in detail, K17 counterstaining with K14 and DAPI was performed. At *Runx1* loss mouse K17 positive periderm cells remained and surrounded K14 positive persistent epithelium (Fig. 7B). At *Cbfb* loss mouse we immunostained other periderm cell marker K6 (Keratin 6) [62]. K6 distribution was evident in wider areas than K17 in the oral epithelium (Fig. 7C). At control mouse, K6 positive periderm was removed from fusion areas, in contrast to remaining periderm layer at *Cbfb* deficient mouse (Fig. 7C).

As cleft etiology in Runx1/Cbfb signaling loss, we detected responsible cause as persistent epithelium located at fusion area between primary and secondary palate. This persistent epithelium was also characterized by disturbed apoptosis and retained proliferation activity. Besides this, periderm removal defect was observed in these mutants.

3. Runx1/Cbfb signaling regulates *Tgfb3* signaling in anterior palate epithelium

Many studies refer the patterning at palate fusion throughout anterior to posterior. This patterning seems to relate with different molecular mechanisms involved in different regions of palate fusion [63]. Among these molecular mechanisms, *Shox2* gene and Msx1-Bmp4-Shh signaling are known to be anterior region specific [16, 25]. To investigate a possible genetic interaction between Runx1/Cbfb signaling and these genes we did gene expression analysis. Whole-mount *in situ* hybridization analysis showed that there is no change at *Shox2, Shh, Bmp4, Msx1* expressions between control and *Runx1* mutant mouse (Fig. 8A). qPCR analysis was also confirmed this (data not shown). Next, we analyzed *Tgfb3* which was intensely studied with isoforms and receptors involved in palate formation. *Tgfb3* null mouse exhibits a complete cleft that effects anterior and posterior area [64]. Epithelial-specific knock out of *Tgfb3* [64], *Tgfbr2* [65] shows milder phenotypes than *Tgfb3* null mouse which demonstrates anterior region cleft. Moreover, *Tgfb3* related cleft pathogenesis includes decreased apoptosis, extensive proliferation and periderm removal deficiency which also overlaps with *Runx1* loss cleft palate etiology [11]. Our analysis demonstrated that *Tgfb3* mRNA expression pattern was similar to *Runx1* which was broadly found at anterior and posterior palate (Fig. 9A). Interestingly *Tgfb3* mRNA expression was disappeared only from primary palate region at Runx1/Cbfb loss mouse (Fig. 9B). In addition, we analyzed mRNA expression pattern of *Mmp13* which is known to be directly induced by *Tgfb3* during palatal fusion [66]. *Mmp13* mRNA expression pattern also overlapped with *Tgfb3* expression at palate (Fig. 9B). Furthermore, the *Mmp13* expression also disappeared from the same region with *Tgfb3* at *Runx1* mutant primary palate (Fig. 9B). qPCR analysis of dissected epithelial tissues from primary palates showed *Tgfb3* and *Mmp13* mRNA expression

loss at *Runx1* mutant mouse (Fig. 9B). As result, Runx1/Cbfb loss mouse demonstrated with significant *Tgfb3* downregulation at primary palate area which coincidences with anterior cleft phenotype.

To confirm whether Runx1-Tgfb3 pathway in primary palate epithelium is crucial for anterior palatogenesis, exogenous TGFB3 was applied at primary palate region of *Runx1* mutants. BSA treated *Runx1* mutant palates were used as the control. TGFB3 protein and BSA treated ex vivo palates were cultured during anterior palate fusion process. TGFB3 protein treated palates demonstrated a fused region between primary and secondary palates while BSA treated mutant palates exhibited a cleft (Fig. 10A). Histological analysis also confirmed mesenchymal confluence at TGFB3 treated palates (Fig. 10A). Approximately 75% of TGFB3 treated mutant palates exhibited fused region (Fig. 10B). To analyze the rescue at gene expressions qPCR analysis were done at TGFB3 and BSA treated mutant palates. *Mmp13* mRNA expression level is increased but such expression was not detected at BSA treated mutant palates (Fig. 10C).

Furthermore, we demonstrated that TGFB3 protein could induce *Runx1* mRNA expression whereas BSA treatment did not induce *Runx1* (Fig. 11A). Sections at bead region also supported *Runx1* mRNA expression around TGFB3 protein soaked beads (Fig. 11A). *Runx1* mRNA expression was not detected at BSA protein implanted region (Fig. 11A). Thus, Runx1-Tgfb3 interaction demonstrated bidirectional relationship at the anterior palate.

Taken together, Runx1/Cbfb signaling is independent with other signaling molecules; *Shh, Shox2, Bmp4, Msx1* that are known to regulate anterior palate fusion. By

contrast, there is anterior region-specific regulation between Runx1/Cbfb signaling and *Tgfb3* which is crucial for anterior palatogenesis.

4. Runx1/Cbfb signaling Stat3 activation at anterior palate formation

Stat3 is one of the important players of Jak/Stat pathway which regulates proliferation, apoptosis, and differentiation. Runx1-Stat3 interaction has been mentioned at epithelial cancer growth and hair cycle regulation [42]. *Runx1* stimulates Stat3 via direct repression of *Socs3* (Suppressor of cytokine signaling-3) in epithelial cancers [55]. However, there is no information about Runx1-Stat3 involvement in palate formation. In order to reveal *Stat3* mRNA expression pattern at palatogenesis, we performed whole-mount *in situ* hybridization at palate formation stages; E14.5 and E15.0. *Stat3* mRNA expression was evident at secondary palate fusion region and palatal shelves in a broad manner at E14.5 stage (Fig. 12A). During fusion between primary palate and secondary palate, *Stat3* mRNA becomes intense at palate fusion areas at both of anterior and posterior (Fig. 12A). Stat3 immunolocalization also overlaps with mRNA expression areas (Fig. 12B). Stat3 immunoreactivity was evident at fusing palate epithelium of both primary and secondary palate, also some signals were evident at mesenchyme at control, *Runx1* and *Cbfb* mutants relatively in similar distribution (Fig. 12B). Phosphorylated Stat3 immunoreactivity was intensely localized at fusing palate epithelium (Fig. 12B). In contrast, we detected pStat3 at *Runx1/Cbfb* mutant remarkably in small areas of primary palate tissue, with no change at secondary palate tissue (Fig. 12B). Western blot analysis was also done to confirm decreased phosphorylated Stat3 at *Runx1* mutants and at *Cbfb* mutants (Fig. 12C).

In order to show possible Socs3 interaction with Runx1-Stat3 activation during palate fusion, we analyze *Socs3* mRNA expression through the whole mount *in situ* and qPCR. Whole mount in situ analysis demonstrated *Socs3* mRNA expression specifically localized at the primary palate, nasal septum area at E14.5 stage (Fig. 13B). At Runx1 mutants, *Socs3* localization was not remarkably changed. However, qPCR analysis detected significant *Socs3* upregulation in *Runx1* mutants (Fig. 13A). Thus, *Runx1* loss leads to *Socs3* upregulation and activated Stat3.

5. Stat3 inhibitor disrupts the anterior palate fusion

In order to reveal Stat3 involvement in palate fusion, we used chemical inhibitors at *in vitr*o culture system. As inhibitors, we use Tyrphostin AG 490 which inhibits JAK2 to block the Stat3 activation pathway [67]. The other inhibitor used is Stat3 inhibitor IV(S3I-201) which inhibits Stat3 activation through diminishing Stat3 phosphorylation [68]. Western blot analysis confirmed decreased pStat3 immunoreactivity at inhibitor-treated primary palate tissues (Fig. 14A). Strikingly inhibitor-treated palates in *in vitro* culture system showed an anterior cleft in high possibility despite proper fusion between primary and secondary palates was proceeded at inhibitor untreated palates (Fig. 14B). Morphological observations demonstrated that the cleft size was directly proportional to the concentration of chemical inhibitor (Fig. 14C). To reveal gene expression deviations at Stat3 inhibitor-treated palates, the qPCR analysis was done. qPCR analysis confirmed dramatic downregulation of *Tgfb3, Mmp13* mRNA expression and *Socs3* upregulation in inhibitor-treated palate tissues correlative with concentration (Fig. 15A). These gene expression deviations are identical with Runx1/Cbfb mutants.

DISCUSSION

In the present study, we demonstrated Runx1/Cbfb signaling deficiency result with the cleft between primary and secondary palates. We revealed improper apoptosis, persistent proliferation in fusing epithelium and periderm removal deficiency as the responsible mechanism for cleft pathogenesis. Moreover, significant *Tgfb3* region specific downregulation is shown as the responsible molecular mechanism of cleft pathogenesis in Runx1/Cbfb mutants. We further demonstrated decreased Stat3 activation and increased *Socs3* expression was evident at fusion areas of *Runx1* mutants. Stat3 inactivation in *in vitro* conditions leads to anterior clefting with decreased *Tgfb3* and upregulated *Socs3* expression which confirmed the Stat3 role in palatogenesis. Altogether these findings indicate that Runx1/Cbfb-Stat3-Tgfb3 as a novel molecular network that regulates palate fusion at the anterior specific region.

1. Role of Runx/Cbfb signaling in anterior palatogenesis

In this study, we used *Cbfb* and *Runx1* epithelium conditional knock out mouse to unclear *Runx* genes role at palatogenesis. We already reported *Runx1* conditional rescued null mouse had an incomplete anterior cleft [26]. The present study using a different genetic background of *Runx1* deficient mouse demonstrated an anterior cleft similar to previous one. The *Runx1* mouse model in the present study is not lethal during the development process. Anterior cleft at survived mouse till adult stage suggests the cleft etiology is not delayed growth. However, Runx genes have the broad expression at palate which includes posterior region. This broad expression did not explain the anterior cleft we got from two *Runx1* mouse models.

This question was answered by using *Cbfb* conditional knockout mouse. *Cbfb* is the predominant partner of *Runx* family proteins. Cbfb forms a heterodimer with *Runxs* and improves their DNA-binding capacity [69]. Mutation of *Cbfb* comprises all *Runx*s transcriptional activity [31]. Owing to this *Cbfb* knockout models exhibits similar phenotypes to *Runx1* or *Runx2* deficient mouse in several tissues [56, 70]. In the present study, *Cbfb* deficient mouse exhibited an anterior cleft similar to previous ones at *Runx1* loss mouse lead us to presume the non-existence of functional redundancy between *Runx* proteins. In addition, the major role of *Runx1* at palatogenesis among *Runx* genes was revealed through using *Runx1* and *Cbfb* deficient mice.

On the other hand, we also demonstrated remarkable *Runx2* and *Runx3* gene expressions at palate during palatogenesis. RUNX2 missense mutations have been shown to cause Cleidocranial Dysplasia (CCD). CCD is an autosomal dominant disorder characterized by skeletal anomalies such as late closure of cranial sutures, late erupting dentition, rudimentary clavicles, and cleft palate [71]. In addition, case studies demonstrated that RUNX2 appears to influence the risk of non-syndromic CLP [72]. Moreover, *Runx2* null mouse embryos exhibited a failure of fusion between the shelves of the secondary palate [73]. From past reports and present findings at *Cbfb* epithelium-specific knock out mouse, we presumed mesenchymal *Runx2* as being an important molecule for secondary palate development. Past studies also showed *Runx3* expression in mouse palate epithelium from E12.5 to E16.5 [74]. However, as far as we know there is no cleft palate phenotype reported with Runx3 molecule mutations in mouse or human.

2. Novel molecular pathway at anterior palatogenesis

Cleft lip palate is very common among human craniofacial malformations and related to multiple genetic and environmental factors. The incidence of CLP in Japan is 1 in 1000, which is considerably high [75]. Treatment can only be done with surgically and often require complex treatments such as speech, dental treatment which continue life-long span. Discovering more about molecular pathways will make the approach to therapies during palatogenesis in an in-utero stage. The recent study showed the intravenous delivery of *Wnt* agonists into pregnant mice restored the *Pax9* loss related cleft of palatal shelves in-utero [17]. In the present study, we reveal new molecular pathway and preliminary rescue data to make an appeal to anterior positioned clefts.

Past studies revealed compromised Tgfb2 signalling in Runx1 loss condition during human embryonic stem cell differentiation [76]. To the best of our knowledge Runx1-Tgfb3 relation was not mentioned in past studies. In the present study, Runx1/Cbfb signaling deficiency results with anterior cleft palate with invariant secondary palate fusion. We also demonstrated striking *Tgfb3* downregulation spatially at the Runx1/Cbfb loss. However, the Tgfb3 promoter does not contain *Runx1* consensus sites within 1kb of the transcription start site [76]. Therefore, there might be some regulating molecule between Runx1/Cbfb and *Tgfb3*.

Tgfb3 is the most investigated gene in CLP studies on the ground of being a critical molecule of the non-syndromic cleft palate in human. Mostly, *Tgfb3* or other *Tgfb* isoforms (*Tgfb1-3*), receptors are widely studied with their cleft palate phenotypes at the mouse. *Tgfb3* null mouse exhibited complete cleft throughout anterior to posterior that is related to *Tgfb3* broad expression. However, deletion of *Tgfb* receptors which are *Alk5* and *Tgfbr2* in the palatal epithelium using K14 promoter

exhibited incomplete clefts at anterior and posterior areas [65, 77]. Moreover, *Tgfb3* loss under K14 promoter demonstrated milder cleft phenotype [64]. Thus, the number of studies mentioned Tgfb signaling involvement in palate fusion with region-specific manner. However, there was no study about *Tgfb3* related anterior specific molecular network or gene. In this study, we claimed the novel molecular network that associated with *Tgfb3* at the only anterior region. Irrelevant from the region, previous studies about Tgfb3 signaling deficiency resulted palatal clefts etiology which contains disturbed apoptosis, persistent proliferation, and periderm removal deficiency. In our study, *Runx1* loss mouse cleft etiology overlaps with *Tgfb3* involved cleft etiologies. This claimed the *Tgfb3* regulating cellular functions during palate fusion at posterior region and anterior region are in a similar way.

Furthermore, past study was successful to recover *Tgfb3* loss resulted cleft via intra-amniotic gene transfer, which has significant importance for therapeutic approaches in human [78]. In our study, we rescue the cleft by exogenous TGFB3 treatment at *in vitro* conditions. According to these results, *Tgfb3* has a substantial role at anterior palate fusion.

It has previously been shown that Tgfb3 signalling was induced *Mmp13* at secondary palates and nasal septum areas[66, 79]. In the present study, we demonstrated decreased expression of *Mmp13* at primary palate region. *Cbfb* deficient mouse showed significant *Mmp13* downregulation at developing femurs [69]. However, *Mmp13* was suggested as target gene of *Runx2* in skeletal tissues [69]. The present study demonstrated *Mmp13* as a target gene of Runx1/Cbfb signaling in anterior palate region.

Present study implied that *Runx1* loss does not lead to alteration of any molecules such as *Shh, Msx1, Bmp4, Shox2* which are known to be deeply involved with

anterior palatogenesis. This indicated that Runx1/Cbfb-Tgfb3 signaling is the novel network which is unrelated to other molecules involved in anterior palate fusion.

3. Stat3 involvement in palatogenesis

Present study first demonstrated *Stat3* expression at palate was very specific at fusion regions at palate development stages. Past study revealed Stat3 inactivation with the Runx1 loss resulted in the impaired growth of cancer [55]. Be associated with past study, we observed decreased Stat3 activation at cleft areas of *Runx1/Cbfb* mutant palates.

STAT3 is the only gene in which pathogenic variants are known to cause autosomal dominant Hyperimmunoglobulin E syndrome (AD-HIES) [80]. Hyperimmunoglobin E Syndrome (HIES) or Job`s syndrome is a rare immunodeficiency with the significant increase in serum immunoglobulin E [81]. HIES case reports showed fibrotic bridges and cavernous clefts on the palate [82]. Furthermore, past study showed STAT1 proteins are strongly expressed in the residual MES of the fusing palate but not the mesenchymal cells and also specifically implicated in promoting apoptosis [83]. However, the possible involvement of other Jak/Stat family members in palate formation has not been elucidated to date. Thus, present study first revealed Stat3 activation existence in the anterior palatogenesis molecular mechanism which is regulated by *Runx1*.

The present evidence at the cleft area with decreased activation of Stat3 exhibited decreased apoptosis which is contradictory to findings in cancer studies. A number of cancer studies implied Stat3 inhibition induced apoptosis at tumor cells. The requirement for deviated Stat3 activity in tumor maintenance and progression

illustrates the Stat3 regulation role of proliferation and apoptosis [84]. However, involution of the mouse mammary gland is characterized by extensive apoptosis of the epithelial cells and the activation of Stat3. *Stat3* deficient mouse exhibited a reduction in epithelial apoptosis and a significant delay of the involution process [85]. Thus, Stat3 regulating cellular functions seem to be tissue specific in diversity.

To reveal further about Runx1-Stat3 activation we analyzed *Socs3* which is an inhibitor of Stat3 [86]. Runx1 is a direct transcriptional repressor of SOCS3 [55]. In our study *Socs3* upregulation was evident at primary palate areas correlated with *Tgfb3* downregulation region. The present findings indicated Runx1-Stat3 activation via repression of *Socs3* directly or indirectly regulates *Tgfb3* expression.

Confirmation of Stat3 role at anterior palatogenesis further is supported by the pharmacological application of Stat3 inhibitors. We use two different Stat3 inhibitors which have different inhibition mechanisms to increase the data accuracy. It should be noted that anterior clefting existed at both of inhibitor-treated palates. Furthermore, *Tgfb3, Mmp13* downregulation, and *Socs3* upregulation were evident in these palates which is same as the *Runx1* mutant. In addition to these gene expression alterations, *Runx1* was also downregulated in inhibitor-treated palates. JAK-STAT signaling pathways seem to be regulated by intrinsic and also environmental factors that support plasticity to the response of a tissue [87]. *Runx1* downregulation demonstrated at present study resulted from Stat3 inhibitor treatment presumed as consequence of Stat3 regulation response to the exogenous factor. This kind of pharmacological modulation of RUNX1 was also suggested as result of cytotoxic agent application [88]. Exogenous factors are well-known etiology of non-syndromic CLP with endogenous factors. Alcohol, tobacco, and drug exposure are well studied exogenous factors [89]. Past studies revealed strong evidence of RUNX2

gene and environmental tobacco smoke association controlling the CLP risk [90]. In according to our results, we suggest that Stat3 may respond to this kind of exogenous factors and regulate gene expression levels. Further studies of Runx1-Stat3 and exogenous factors relation in CLP pathology would be of value to the therapeutic approaches.

In the present study, we had a limitation that data analysis could not be done with the mouse with *Stat3* loss genetic background. Previous studies showed *Stat3* significance during embryogenesis with using the *Stat3* deficient mouse which is lethal at early stages [91]. In future experiments, we are going to generate tissue-specific *Stat3* knock out mouse to confirm our study and further reveal detailed roles of *Stat3* in palatogenesis.

ACKNOWLEDGEMENTS

Firstly, I would like to express my sincere gratitude to my advisor Prof. Yamashiro for the continuous support of my PhD study and related research. I also appreciate him for making me motivated about my research and research career. In his busy schedule, I always had a time to discussing my study or other researches. His guidance and education system always made me think more, study more and do experiments more.

My sincere thanks also go to Dr. Kurosaka for the stimulating discussions and teaching for experiment methods. Without his support and contributions, I would not have been possible to continue this study. I am also grateful to Dr. Mihara for teaching me experiment methods and supporting me for my study. I am highly indebted and thoroughly grateful to Dr. Ono-Minagi for her continuous support and encouraging me for my research.

I would also like to express my thanks to Mrs. Nogami for her skills and supports at experiments and sample collection. Also, I owe a deep gratitude to Mrs. Yasutake for teaching me basic experiment skills at my really first experience at researches.

A very special gratitude goes out to all down at Japanese Government (Monbukagakusho) Scholarship for supporting me for four years during my PhD education.

And finally, last but not the least, I would like to thank my family and my friends for supporting me spiritually throughout doing researches and my life in general.

ABBREVIATIONS

CLP	Cleft lip and/or palate
RUNX	Runt related transcription factor
CBFB	Core-binding factor subunit beta
LG	Lacrimal gland
HF	Hair follicle
SMG	Submandibular gland
TGFB	Transforming Growth Factor-Beta
JAK-STAT	Janus Kinase/Signal Transducer and Activator of Transcription
STAT	Signal Transducer and Activator of Transcription
JAK	Janus Kinase
TYK	Tyrosine Kinase
MES	Midline epithelial seam
SHH	Sonic Hedgehog
SHOX2	Short Stature Homeobox 2
MSX1	Msh homeobox1
BMP4	Bone-morphogenetic protein 4
FGF10	Fibroblast Growth Factor 10
GAPDH	Glyceraldehyde 3-phosphate dehydrogenase
SOCS	Suppressor of cytokine signaling
BSA	Bovine Serum Albumin
MMP	Matrix metalloproteinase
TGFBR	Transforming Growth Factor beta receptor
HIES	Hyperimmunoglobulin E syndrome
CCD	Cleidocranial Dysplasia

REFERENCES

1. Francis-West P, Crespo-Enriquez I. Vertebrate Embryo: Craniofacial Development. eLS: John Wiley & Sons, Ltd; 2001.
2. Jiang R, Bush JO, Lidral AC. Development of the upper lip: morphogenetic and molecular mechanisms. Dev Dyn. 2006;235:1152-1166.
3. Ferguson MW. Palate development. Development. 1988;103 Suppl:41-60.
4. Bush JO, Jiang RL. Palatogenesis: morphogenetic and molecular mechanisms of secondary palate development (vol 139, pg 231, 2012). Development. 2012;139:828-828.
5. Gritli-Linde A. Molecular control of secondary palate development. Dev Biol. 2007;301:309-326.
6. Cuervo R, Covarrubias L. Death is the major fate of medial edge epithelial cells and the cause of basal lamina degradation during palatogenesis. Development. 2004;131:15.
7. Martinez-Alvarez C, Blanco MJ, Perez R, et al. Snail family members and cell survival in physiological and pathological cleft palates. Dev Biol. 2004;265:207-218.
8. Vaziri Sani F, Hallberg K, Harfe BD, et al. Fate-mapping of the epithelial seam during palatal fusion rules out epithelial-mesenchymal transformation. Dev Biol. 2005;285:490-495.
9. Funato N, Nakamura M, Richardson JA, et al. Tbx1 regulates oral epithelial adhesion and palatal development. Human Molecular Genetics. 2012;21:2524-2537.
10. Richardson RJ, Hammond NL, Coulombe PA, et al. Periderm prevents pathological epithelial adhesions during embryogenesis. The Journal of Clinical Investigation. 2014;124:3891-3900.
11. Richardson R, Mitchell K, Hammond NL, et al. p63 exerts spatio-temporal control of palatal epithelial cell fate to prevent cleft palate. PLOS Genetics. 2017;13:e1006828.
12. Johnston MC, Bronsky PT. Prenatal craniofacial development: new insights on normal and abnormal mechanisms. Crit Rev Oral Biol Med. 1995;6:368-422.
13. Stuppia L, Capogreco M, Marzo G, et al. Genetics of syndromic and nonsyndromic cleft lip and palate. J Craniofac Surg. 2011;22:1722-1726.
14. Cobourne MT, Xavier GM, Depew M, et al. Sonic hedgehog signalling inhibits palatogenesis and arrests tooth development in a mouse model of the nevoid basal cell carcinoma syndrome. Developmental Biology. 2009;331:38-49.
15. Yang L-T, Kaartinen V. Tgfb1 expressed in the Tgfb3 locus partially rescues the cleft palate phenotype of Tgfb3 null mutants. Developmental biology. 2007;312:384-395.
16. Yu L, Gu S, Alappat S, et al. Shox2-deficient mice exhibit a rare type of incomplete clefting of the secondary palate. Development. 2005;132:4397-4406.
17. Jia S, Zhou J, Fanelli C, et al. Small-molecule Wnt agonists correct cleft palates in Pax9 mutant mice in utero. Development. 2017;144:3819-3828.
18. Rice R, Spencer-Dene B, Connor EC, et al. Disruption of Fgf10/Fgfr2b-coordinated epithelial-mesenchymal interactions causes cleft palate. The Journal of Clinical Investigation.

2004;113:1692-1700.
19. Kaartinen V, Voncken JW, Shuler C, et al. Abnormal lung development and cleft palate in mice lacking TGF-beta 3 indicates defects of epithelial-mesenchymal interaction. Nat Genet. 1995;11:415-421.
20. Brunet CL, Sharpe PM, Ferguson MW. Inhibition of TGF-beta 3 (but not TGF-beta 1 or TGF-beta 2) activity prevents normal mouse embryonic palate fusion. Int J Dev Biol. 1995;39:345-355.
21. Taya Y, O'Kane S, Ferguson MW. Pathogenesis of cleft palate in TGF-beta3 knockout mice. Development. 1999;126:3869-3879.
22. Lidral AC, Romitti PA, Basart AM, et al. Association of MSX1 and TGFB3 with nonsyndromic clefting in humans. Am J Hum Genet. 1998;63:557-568.
23. Zhu J, Hao L, Li S, et al. MTHFR, TGFB3, and TGFA polymorphisms and their association with the risk of non-syndromic cleft lip and cleft palate in China. American Journal of Medical Genetics Part A. 2010;152A:291-298.
24. Ichikawa E, Watanabe A, Nakano Y, et al. PAX9 and TGFB3 are linked to susceptibility to nonsyndromic cleft lip with or without cleft palate in the Japanese: population-based and family-based candidate gene analyses. Journal Of Human Genetics. 2005;51:38.
25. Zhang ZY, Song YQ, Zhao X, et al. Rescue of cleft palate in Msx1-deficient mice by transgenic Bmp4 reveals a network of BMP and Shh signaling in the regulation of mammalian palatogenesis. Development. 2002;129:4135-4146.
26. Charoenchaikorn K, Yokomizo T, Rice DP, et al. Runx1 is involved in the fusion of the primary and the secondary palatal shelves. Developmental Biology. 2009;326:392-402.
27. Ito Y. RUNX Genes in Development and Cancer: Regulation of Viral Gene Expression and the Discovery of RUNX Family Genes. Advances in Cancer Research: Academic Press; 2008:33-76.
28. Browne G, Taipaleenmaki H, Bishop NM, et al. Runx1 is associated with breast cancer progression in MMTV-PyMT transgenic mice and its depletion in vitro inhibits migration and invasion. J Cell Physiol. 2015;230:2522-2532.
29. Ferrari N, McDonald L, Morris JS, et al. RUNX2 in mammary gland development and breast cancer. J Cell Physiol. 2013;228:1137-1142.
30. Lotem J, Levanon D, Negreanu V, et al. Runx3 in Immunity, Inflammation and Cancer. Adv Exp Med Biol. 2017;962:369-393.
31. Komori T. The functions of Runx family transcription factors and Cbfb in skeletal development. Oral Science International. 2015;12:1-4.
32. Levanon D, Negreanu V, Bernstein Y, et al. AML1, AML2, and AML3, the human members of the runt domain gene-family: cDNA structure, expression, and chromosomal localization. Genomics. 1994;23:425-432.
33. Kimura A, Inose H, Yano F, et al. Runx1 and Runx2 cooperate during sternal morphogenesis. Development. 2010;137:1159-1167.
34. Smith N, Dong Y, Lian JB, et al. Overlapping expression of Runx1(Cbfa2) and Runx2(Cbfa1) transcription factors supports cooperative induction of skeletal development. Journal of Cellular Physiology. 2005;203:133-143.

35. Yoshida CA, Yamamoto H, Fujita T, et al. Runx2 and Runx3 are essential for chondrocyte maturation, and Runx2 regulates limb growth through induction of Indian hedgehog. Genes Dev. 2004;18:952-963.
36. Kurosaka H, Islam MN, Kuremoto K, et al. Core binding factor beta functions in the maintenance of stem cells and orchestrates continuous proliferation and differentiation in mouse incisors. Stem Cells. 2011;29:1792-1803.
37. Ono Minagi H, Sarper SE, Kurosaka H, et al. Runx1 mediates the development of the granular convoluted tubules in the submandibular glands. PLOS ONE. 2017;12:e0184395.
38. Voronov D, Gromova A, Liu D, et al. Transcription factors Runx1 to 3 are expressed in the lacrimal gland epithelium and are involved in regulation of gland morphogenesis and regeneration. Invest Ophthalmol Vis Sci. 2013;54:3115-3125.
39. Islam MN, Itoh S, Yanagita T, et al. Runx/Cbfb signaling regulates postnatal development of granular convoluted tubule in the mouse submandibular gland. Developmental Dynamics. 2015;244:488-496.
40. D'Souza RN, Aberg T, Gaikwad J, et al. Cbfa1 is required for epithelial-mesenchymal interactions regulating tooth development in mice. Development. 1999;126:2911-2920.
41. Glotzer DJ, Zelzer E, Olsen BR. Impaired skin and hair follicle development in Runx2 deficient mice. Developmental Biology. 2008;315:459-473.
42. Osorio KM, Lilja KC, Tumbar T. Runx1 modulates adult hair follicle stem cell emergence and maintenance from distinct embryonic skin compartments. The Journal of Cell Biology. 2011;193:235-250.
43. Gaidzik VI, Bullinger L, Schlenk RF, et al. RUNX1 Mutations in Acute Myeloid Leukemia: Results From a Comprehensive Genetic and Clinical Analysis From the AML Study Group. Journal of Clinical Oncology. 2011;29:1364-1372.
44. Braddock SR, South ST, Schiffman JD, et al. Braddock-Carey syndrome: A 21q22 contiguous gene syndrome encompassing RUNX1. Am J Med Genet A. 2016;170:2580-2586.
45. Liu P, Tarle SA, Hajra A, et al. Fusion between transcription factor CBF beta/PEBP2 beta and a myosin heavy chain in acute myeloid leukemia. Science. 1993;261:1041-1044.
46. Goto T, Aramaki M, Yoshihashi H, et al. Large fontanelles are a shared feature of haploinsufficiency of RUNX2 and its co-activator CBFB. Congenital Anomalies. 2004;44:225-229.
47. Khan A, Hyde RK, Dutra A, et al. Core binding factor beta (CBFB) haploinsufficiency due to an interstitial deletion at 16q21q22 resulting in delayed cranial ossification, cleft palate, congenital heart anomalies, and feeding difficulties but favorable outcome. American Journal of Medical Genetics Part A. 2006;140A:2349-2354.
48. Rawlings JS, Rosler KM, Harrison DA. The JAK/STAT signaling pathway. Journal of Cell Science. 2004;117:1281.
49. Sano S, Itami S, Takeda K, et al. Keratinocyte-specific ablation of Stat3 exhibits impaired skin remodeling, but does not affect skin morphogenesis. Embo j. 1999;18:4657-4668.
50. Takeda K, Clausen BE, Kaisho T, et al. Enhanced Th1 activity and development of chronic enterocolitis in mice devoid of Stat3 in macrophages and neutrophils. Immunity. 1999;10:39-49.

51. Chapman RS, Lourenco PC, Tonner E, et al. Suppression of epithelial apoptosis and delayed mammary gland involution in mice with a conditional knockout of Stat3. Genes Dev. 1999;13:2604-2616.
52. Akira S. Roles of STAT3 defined by tissue-specific gene targeting. Oncogene. 2000;19:2607.
53. Williams JG. STAT signalling in cell proliferation and in development. Current Opinion in Genetics & Development. 2000;10:503-507.
54. Yu H, Lee H, Herrmann A, et al. Revisiting STAT3 signalling in cancer: new and unexpected biological functions. Nature Reviews Cancer. 2014;14:736.
55. Scheitz CJF, Lee TS, McDermitt DJ, et al. Defining a tissue stem cell-driven Runx1/Stat3 signalling axis in epithelial cancer. The EMBO Journal. 2012;31:4124-4139.
56. Wang Q, Stacy T, Miller JD, et al. The CBFβ Subunit Is Essential for CBFα2 (AML1) Function In Vivo. Cell. 1996;87:697-708.
57. Soriano P. Generalized lacZ expression with the ROSA26 Cre reporter strain. Nature Genetics. 1999;21:70.
58. Nomir AG, Takeuchi Y, Fujikawa J, et al. Fate mapping of Trps1 daughter cells during cardiac development using novel Trps1-Cre mice. genesis. 2016;54:379-388.
59. Yamashiro T, Åberg T, Levanon D, et al. Expression of Runx1, -2 and -3 during tooth, palate and craniofacial bone development. Mechanisms of Development. 2002;119:S107-S110.
60. Ito Y, Bae S-C, Chuang LSH. The RUNX family: developmental regulators in cancer. Nature Reviews Cancer. 2015;15:81.
61. Cecconi F, Alvarez-Bolado G, Meyer BI, et al. Apaf1 (CED-4 homolog) regulates programmed cell death in mammalian development. Cell. 1998;94:727-737.
62. Hammond NL, Dixon J, Dixon MJ. Periderm: Life-cycle and function during orofacial and epidermal development. Seminars in Cell & Developmental Biology. 2017.
63. Hilliard SA, Yu L, Gu S, et al. Regional regulation of palatal growth and patterning along the anterior-posterior axis in mice. J Anat. 2005;207:655-667.
64. Lane J, Yumoto K, Pisano J, et al. Control elements targeting Tgfb3 expression to the palatal epithelium are located intergenically and in introns of the upstream Ift43 gene. Frontiers in Physiology. 2014;5:258.
65. Xu X, Han J, Ito Y, et al. Cell autonomous requirement for Tgfbr2 in the disappearance of medial edge epithelium during palatal fusion. Dev Biol. 2006;297:238-248.
66. Blavier L, Lazaryev A, Groffen J, et al. TGF-β3-induced Palatogenesis Requires Matrix Metalloproteinases. Molecular Biology of the Cell. 2001;12:1457-1466.
67. Seo IA, Lee HK, Shin YK, et al. Janus Kinase 2 Inhibitor AG490 Inhibits the STAT3 Signaling Pathway by Suppressing Protein Translation of gp130. The Korean Journal of Physiology & Pharmacology : Official Journal of the Korean Physiological Society and the Korean Society of Pharmacology. 2009;13:131-138.
68. Pang M, Ma L, Gong R, et al. A novel STAT3 inhibitor, S3I-201, attenuates renal interstitial fibroblast activation and interstitial fibrosis in obstructive nephropathy. Kidney International. 2010;78:257-268.
69. Qin X, Jiang Q, Matsuo Y, et al. Cbfb regulates bone development by stabilizing Runx family

proteins. J Bone Miner Res. 2015;30:706-714.
70. Chen W, Ma J, Zhu G, et al. Cbfbeta deletion in mice recapitulates cleidocranial dysplasia and reveals multiple functions of Cbfbeta required for skeletal development. Proc Natl Acad Sci U S A. 2014;111:8482-8487.
71. Otto F, Kanegane H, Mundlos S. Mutations in the RUNX2 gene in patients with cleidocranial dysplasia. Hum Mutat. 2002;19:209-216.
72. Sull JW, Liang K-Y, Hetmanski JB, et al. Differential Parental Transmission of Markers in RUNX2 Among Cleft Case-Parent Trios From Four Populations. Genetic epidemiology. 2008;32:505-512.
73. Aberg T, Cavender A, Gaikwad JS, et al. Phenotypic changes in dentition of Runx2 homozygote-null mutant mice. J Histochem Cytochem. 2004;52:131-139.
74. Yamamoto H, Ito K, Kawai M, et al. Runx3 expression during mouse tongue and palate development. The Anatomical Record Part A: Discoveries in Molecular, Cellular, and Evolutionary Biology. 2006;288A:695-699.
75. Natsume N, Kawai T, Kohama G, et al. Incidence of cleft lip or palate in 303738 Japanese babies born between 1994 and 1995. British Journal of Oral and Maxillofacial Surgery. 2000;38:605-607.
76. VanOudenhove Jennifer J, Medina R, Ghule Prachi N, et al. Transient RUNX1 Expression during Early Mesendodermal Differentiation of hESCs Promotes Epithelial to Mesenchymal Transition through TGFB2 Signaling. Stem Cell Reports. 2016;7:884-896.
77. Dudas M, Kim J, Li WY, et al. Epithelial and ectomesenchymal role of the type I TGF-beta receptor ALK5 during facial morphogenesis and palatal fusion. Dev Biol. 2006;296:298-314.
78. Wu C, Endo M, Yang BH, et al. Intra-amniotic Transient Transduction of the Periderm With a Viral Vector Encoding TGF[beta]3 Prevents Cleft Palate in Tgf[beta]3-/- Mouse Embryos. Mol Ther. 2013;21:8-17.
79. Lane J, Yumoto K, Azhar M, et al. Tak1, Smad4 and Trim33 redundantly mediate TGF-β3 signaling during palate development. Developmental Biology. 2015;398:231-241.
80. Hsu AP, Davis J, Puck JM, et al. Autosomal Dominant Hyper IgE Syndrome. In: Adam MP, Ardinger HH, Pagon RA, et al., eds. GeneReviews((R)). Seattle (WA): University of Washington, Seattle University of Washington, Seattle. GeneReviews is a registered trademark of the University of Washington, Seattle. All rights reserved.; 1993.
81. James J, Thekkeveetil AK, Vadakkepurayil K. Oral Manifestations of Job's Syndrome in a Paediatric Dental Patient – A Case Report. Journal of Clinical and Diagnostic Research : JCDR. 2016;10:ZD04-ZD05.
82. Domingo DL, Freeman AF, Davis J, et al. Novel intraoral phenotypes in hyperimmunoglobulin-E syndrome. Oral Diseases. 2008;14:73-81.
83. Britto JA, Evans RD, Hayward RD, et al. Toward pathogenesis of Apert cleft palate: FGF, FGFR, and TGF beta genes are differentially expressed in sequential stages of human palatal shelf fusion. Cleft Palate Craniofac J. 2002;39:332-340.
84. Siddiquee KAZ, Turkson J. STAT3 as a target for inducing apoptosis in solid and hematological tumors. Cell research. 2008;18:254-267.

85. Chapman RS, Lourenco P, Tonner E, et al. The role of Stat3 in apoptosis and mammary gland involution. Conditional deletion of Stat3. Adv Exp Med Biol. 2000;480:129-138.
86. Carow B, Rottenberg ME. SOCS3, a Major Regulator of Infection and Inflammation. Frontiers in Immunology. 2014;5:58.
87. Aaronson DS, Horvath CM. A Road Map for Those Who Don't Know JAK-STAT. Science. 2002;296:1653.
88. Speidel D, Wellbrock J, Abas M. RUNX1 upregulation by cytotoxic drugs promotes apoptosis. Cancer Research. 2017.
89. Kawalec A, Nelke K, Pawlas K, et al. Risk factors involved in orofacial cleft predisposition – review. Open Medicine. 2015;10:163-175.
90. Wu T, Fallin MD, Shi M, et al. Evidence of Gene-Environment Interaction for the RUNX2 Gene and Environmental Tobacco Smoke in Controlling the Risk of Cleft Lip with/without Cleft Palate. Birth defects research. Part A, Clinical and molecular teratology. 2012;94:76-83.
91. Takeda K, Noguchi K, Shi W, et al. Targeted disruption of the mouse Stat3 gene leads to early embryonic lethality. Proc Natl Acad Sci U S A. 1997;94:3801-3804.

FIGURE LEGENDS

Figure 1 K14-Cre/*Runx1*$^{fl/fl}$ and K14-Cre/*Cbfb*$^{fl/fl}$ mutants exhibit anterior region cleft palate

A: X gal stained frontal sections from the primary and secondary palate of demonstrating positive staining at oral epithelium areas. The section from primary palate area from E15.0 embryos displays positive staining at fusion epithelium between primary and secondary palates (arrowheads). Secondary palate area section showed positive staining at midline epithelial seam (arrowheads). pp, primary palate; sp, secondary palate; ns, nasal septum. Scale bar = 200 µm.

B: Occlusal views of control palate at P0 and P50 displayed fusion between primary palate and secondary palate leaving two small holes, anatomically known as orifice of incisive canal (oi). At K14-Cre/*Runx1*$^{fl/fl}$ and K14-Cre/*Cbfb*$^{fl/fl}$ mutant cleft was observed between primary and secondary palate, while the secondary palate completely fused (arrowheads). At P50, First and second rugaes proper fusion between two secondary palates were disturbed at K14-Cre/Runx1$^{fl/fl}$ and K14-Cre/Cbfb$^{fl/fl}$ (arrows). pp, primary palate; sp, secondary palate; oi, orifices of incisive canal. Scale bar = 500 µm.

C: Table shows control and mutants phenotype incidence.

Figure 2 Expression patterns of *Runx1, Runx2, Runx3* and *Cbfb* mRNA during palatogenesis

A: *Runx1* mRNA expression at E14.0 is detected at incisors, rugaes, secondary palate shelves, primary palate-nasal septum area. At E15.0, *Runx1* mRNA is highly expressed at the secondary palate, primary palate fusion areas. Strong expression of *Runx1* was seen at primary palate area (arrowheads). Unique expression pattern around orifice of incisive canal was detected at *Runx1* mRNA stained palates (*). *Runx2* mRNA expression at E14.0 is detected at incisors, rugaes, palate shelves and nasal septum-primary palate area. At E15.0 *Runx2* mRNA expressed abundantly at fusing palate areas. *Runx3* mRNA expression exhibited similar with *Runx2*, with a broad expression of palate shelves and nasal septum. *Cbfb* mRNA expression at E14.0 and E15.0 is detected throughout at palate areas and incisor. pp, primary palate; sp, secondary palate; oi, orifices of incisive canal; ns, nasal septum. Scale bar = 1000 μm.

Figure 3 Palatal growth defect was not found at Runx1/Cbfb loss mouse

A: Occlusal views of palates of control and K14-Cre/*Runx1*$^{fl/fl}$ at E15.0, before anterior region fusion. Palatal tissue processes appeared as similar size at control and K14-Cre/*Runx1*$^{fl/fl}$. Dashed white lines encircled orifices of incisive canal. pp, primary palate; sp, secondary palate; oi, orifices of incisive canal; ru, rugae. Scale bar = 200 μm.

B: Schematic drawing of the palate and blue lines show the position of the sections. pp, primary palate; sp, secondary palate.

C: BrdU staining (brown) of control and K14-Cre/*Runx1*$^{fl/fl}$ mice at E15.0. A section through the anterior region of the palate and fusion area shows a similar level of cell proliferation. pp, primary palate; sp, secondary palate. Scale bar = 100 μm.

Figure 4 Run1/Cbfb deficient mouse failed fusion between primary and secondary palate; nasal septum and secondary palate at posterior areas

A: Histological examination of anterior palate section reveals a failure of fusion between the primary and secondary palate in the Runx1/Cbfb deficient mice at E17.0 (arrows). Sections from more posterior area exhibit a gap between nasal septum and secondary palate (*). pp, primary palate; sp, secondary palate; ns, nasal septum. Scale bar = 200 μm.

B: K14 immunostained (red) fusion area epithelium was disappeared from fusion areas at control (arrow). At Runx1/Cbfb deficient mouse K14 positive epithelium remained at fusion areas. pp, primary palate; sp, secondary palate. Scale bar = 100 μm.

Figure 5 Apoptosis was critically decreased at Runx1/Cbfb loss mouse fusion areas

A: A section through the anterior palate shelf of E15.0 mutant (arrow) shows a lower level of cell apoptosis compared to control (arrowhead). The section from posterior palate shows a similar level of cell death. The graph shows a comparison of TUNEL positive cell number in fusion region. The analyses were repeated at least three times using three mice each of control and mutant. Data were normalized by the

amount of TUNEL positive cell at control. pp, primary palate; sp, secondary palate. Scale bar = 100 µm.

Figure 6 *Runx1, Cbfb* mutant epithelium showed persistent proliferation

A: K14 (red), Ki67 (green) double-stained sections from fusion areas exhibited Ki67 positive proliferating cells in fusing epithelium of *Runx1* deficient mouse (arrowheads). The graph shows the significant increase in the percentage of proliferative cells in the epithelium of Runx1/Cbfb deficient mouse compared to control mouse. The analyses were repeated at least three times using three mice each of control and mutant. pp, primary palate; sp, secondary palate. Scale bar = 50 µm.

Figure 7 *Runx1* and *Cbfb* deficiency resulted in resistant periderm layer

A: K17 (green) positive periderm cells disappeared from fusion region of the control mouse (arrowhead). At *Runx1* loss mouse periderm cells retained between primary and secondary palates (arrows). pp, primary palate; sp, secondary palate. Scale bar = 100 µm.

B: The closer image of mutant palate fusion region double-stained K14 (red) and K17 (green) demonstrated periderm cover the persistent epithelium. pp, primary palate; sp, secondary palate. Scale bar = 75 µm.

C: Other periderm marker K6 (green) immunostained sections showed removal from fusion region of the control mouse (arrowhead). At *Cbfb* loss mouse periderm cells

retained between primary and secondary palates (arrows). pp, primary palate; sp, secondary palate. Scale bar = 100 μm.

Figure 8 *Runx1* loss was not affected *Shh, Msx1, Shox2, Bmp4* gene expressions.

A: Whole-mount *in situ* hybridization analysis of *Shh, Msx1, Shox2, Bmp4* at control and *Runx1* deficient mouse. No significant difference was found in gene expression patterns. pp, primary palate; sp, secondary palate; oi, orifices of incisive canal. Scale bar = 500 μm.

Figure 9 *Tgfb3* regional downregulation was detected in Runx1/Cbfb mutant mouse

A: At E15.0 stage, *Tgfb3* mRNA expression is detected at fusion regions at primary and secondary palates in control mouse. At Runx1/Cbfb deficient mouse, *Tgfb3* expression disappeared from primary palate region though existence at the secondary palate. pp, primary palate; sp, secondary palate; oi, orifices of incisive canal. Scale bar = 500 μm.

B: Closer images of *Tgfb3* expression at primary palate of control and *Runx1* loss mouse. *Tgfb3* and *Mmp13* expressions disappeared from primary palate area of the *Runx1* mutant mouse (arrowheads). qPCR analysis showed significant decreased *Tgfb3* and *Mmp13* expression in *Runx1* loss mouse primary palate epithelium. The quantification was normalized to *Gapdh.* The qPCR analyses were repeated at least three times using three mice each of control and mutant. Dashed white lines encircled orifices of incisive canal. pp, primary palate; sp, secondary palate; oi, orifices of incisive canal. Scale bar = 500 μm.

Figure 10 Exogenous TGFB3 rescued the cleft at *Runx1* loss mouse

A: Morphological analysis demonstrated cleft at BSA treated *Runx1* mutant palate and fusion area at TGFB3 treated palates. Histological section from fusion area confirmed a fusion at TGFB3 treated palates. Dashed white lines encircled orifices of incisive canal. pp, primary palate; sp, secondary palate. Scale bar = 100 μm.

B: Table shows the percentage of anterior palate fusion occurrence.

C: qPCR analysis shows restored *Mmp13* expression in TGFB3 treated tissues. The quantification was normalized to *Gapdh.*

Figure 11 Runx1-Tgfb3 relation is bidirectional at primary palate tissue

A: Whole-mount *in situ* analysis of *Runx1* expression at BSA and TGFB3 treated palates. *Runx1* mRNA expression was evident around TGFB3 bead explanted area. Histological sections at BSA and TGFB3 treated areas also show induced *Runx1* expression around the TGFB3 treated bead. Blue oval indicates TGFB3 or BSA bead. pp, primary palate; sp, secondary palate. Scale bar = 200 μm.

Figure 12 Runx1/Cbfb deficiency leads to decreased activity of Stat3

A: *Stat3* mRNA expression at the E14.5 stage is broad at anterior-posterior aspect. At E15.0 *Stat3* expression become intense at fusion areas. pp, primary palate; sp, secondary palate; oi, orifices of incisive canal. Scale bar = 500 μm.

B: Stat3 (green) immunoreactivity was evident at epithelium of fusion areas (arrowheads), some signals also appeared on mesenchyme. Stat3 immunoreactive

localization was not significantly changed at the Runx1/Cbfb mutant mouse. pStat3 (green) was detected at fusing epithelium areas at primary and secondary palates (arrows). Runx1/Cbfb mutants showed significant loss of pStat3 at the primary palate, though some signals were detected at secondary palates (*). pp, primary palate; sp, secondary palate. Scale bar = 100 μm.

C: Western blot analysis showed decreased pStat3 immunoreactivity at primary palate tissue of Runx1/Cbfb loss mouse.

Figure 13 *Socs3* upregulation was detected at the *Runx1* loss.

A: qPCR analysis showed significant upregulation of *Socs3* in *Runx1* mutant mouse primary palate epithelium. The quantification was normalized to *Gapdh.* The qPCR analyses were repeated at least three times using three mice each of control and mutant.

B: Whole-mount *in situ* expression of the palate at E14.5 stage demonstrated *Socs3* upregulation areas at the *Runx1* mutant. At same stage, *Tgfb3* downregulation was detected where overlaps with *Socs3* upregulation areas. Dashed white lines encircled orifices of incisive canal. pp, primary palate; sp, secondary palate; oi, orifices of incisive canal. Scale bar = 100 μm.

Figure 14 Stat3 chemical inhibitors treated palates resulted in anterior cleft

A: Western blot analysis revealed decreased pStat3 immunoreactivity at AG490 and S3I-201 treated primary palate tissues.

B: Table shows frequency of anterior cleft of control and AG490 and S3I-201 treated *ex vivo* palates.

C: Morphological analysis showed proper fusion at control and cleft at AG490 and S3I-201 treated palates. Dashed white lines encircled orifices of incisive canal. pp, primary palate; sp, secondary palate; oi, orifices of incisive canal. Scale bar = 250 µm.

Figure 15 Stat3 inhibitor-treated palates demonstrated *Tgfb3, Mmp13* downregulation, and *Socs3* upregulation

A: qPCR analysis revealed *Tgfbf3, Mmp13, Runx1* downregulation and *Socs3* upregulation at AG490 treated palates in different concentration. The quantification was normalized to *Gapdh.* The qPCR analyses were repeated at least three times using three mice each of control and mutant.

B: qPCR analysis revealed *Tgfbf3, Mmp13, Runx1* downregulation and *Socs3* upregulation at S3I-201 treated palates in different concentration. The quantification was normalized to *Gapdh.* The qPCR analyses were repeated at least three times using three mice each of control and mutant.

Figure 16 Runx1/Cbfb-Stat3-Tgfb3 signaling axis is regulating anterior palatogenesis.

Runx1/Cbfb deficiency leads to *Socs3* upregulation and decreased Stat3 activation. Further *Tgfb3* is downregulated in primary palate area. These gene expression

deviations in Runx1/Cbfb loss lead the cleft between primary and secondary palates. Runx1/Cbfb and Tgfb3 relation is bidirectional manner. Exogenous TGFB3 application at Runx1 null condition rescue the anterior cleft. Pharmacological inhibition of Stat3 in wild-type exhibited gene expression deviations similar tendency with Runx1/Cbfb loss condition. Moreover, inhibitor-treated palates demonstrated anterior cleft.

Figure 17 Primer Sequences used for quantitive PCR and for probe generation

A

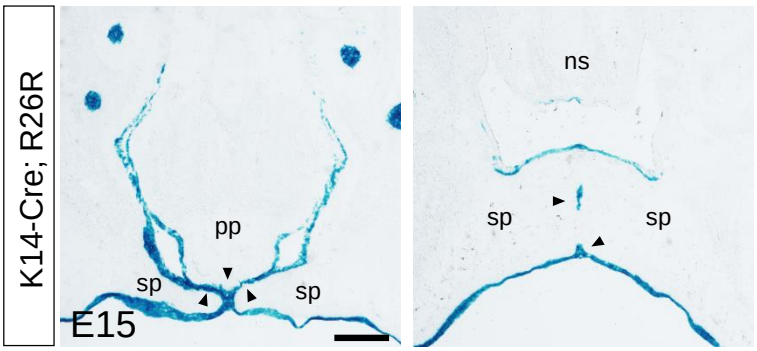

B

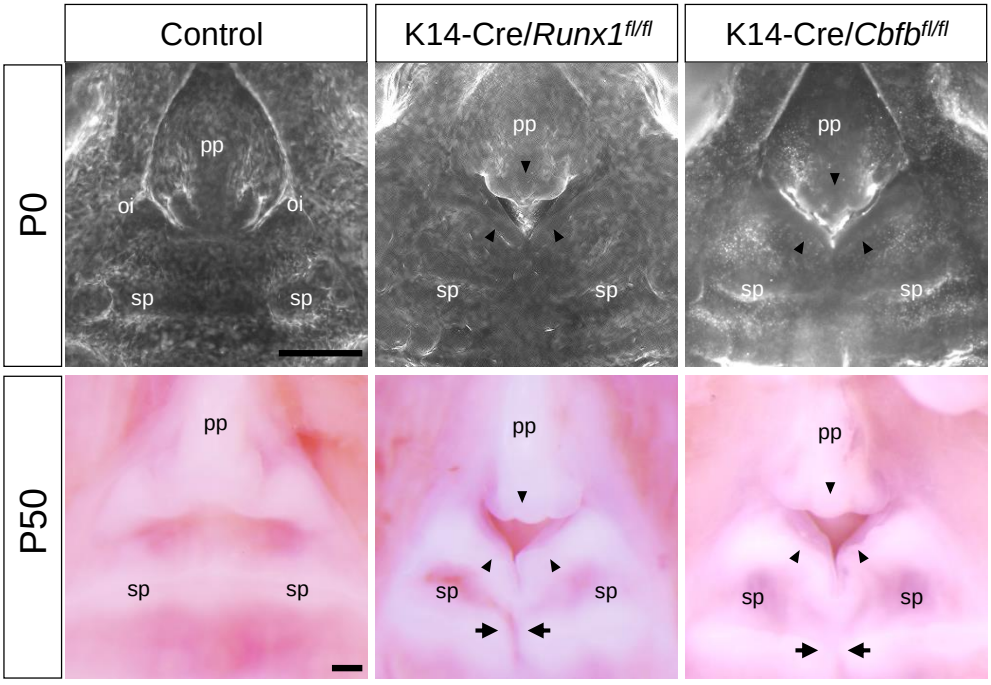

C

Frequency of anterior cleft		
Genotype	Frequency	
Control	0%	(0/13)
K14-Cre/*Runx1*$^{fl/fl}$	92%	(12/13)
K14-Cre/*Cbfb*$^{fl/fl}$	100%	(8/8)

Figure 1

A

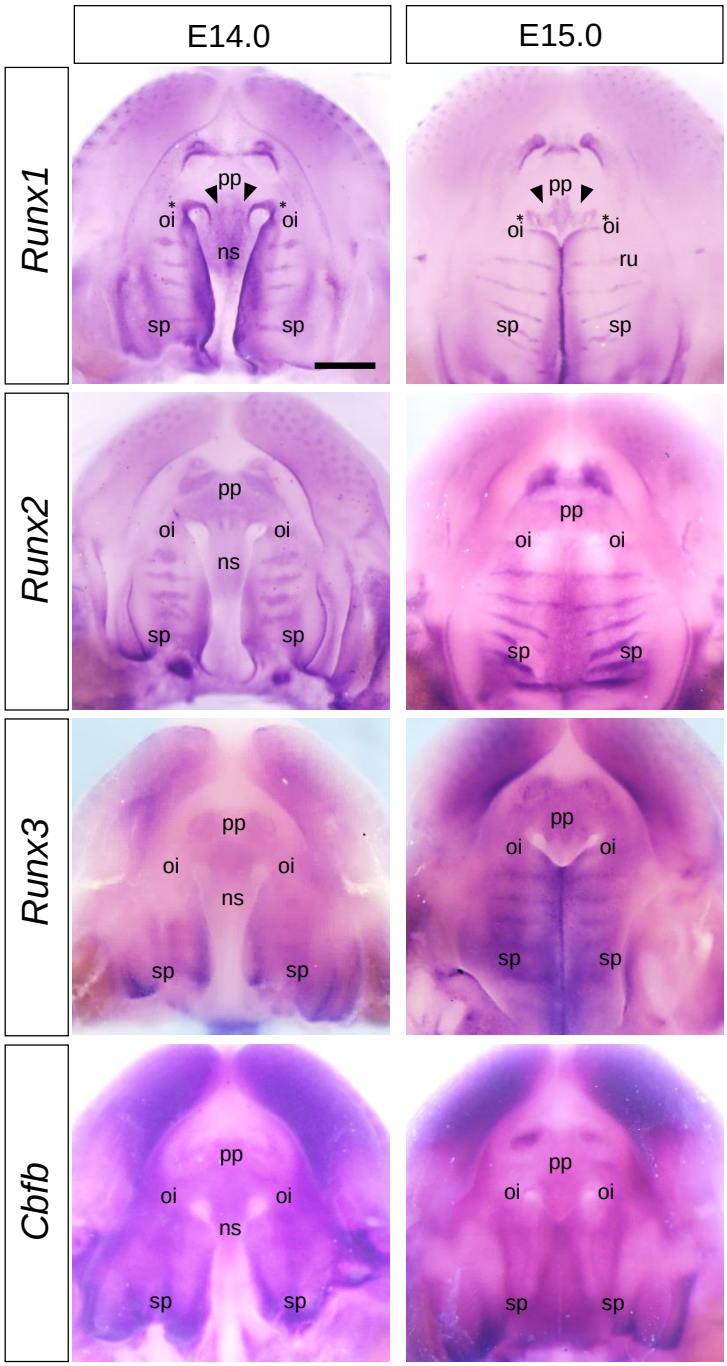

Figure 2

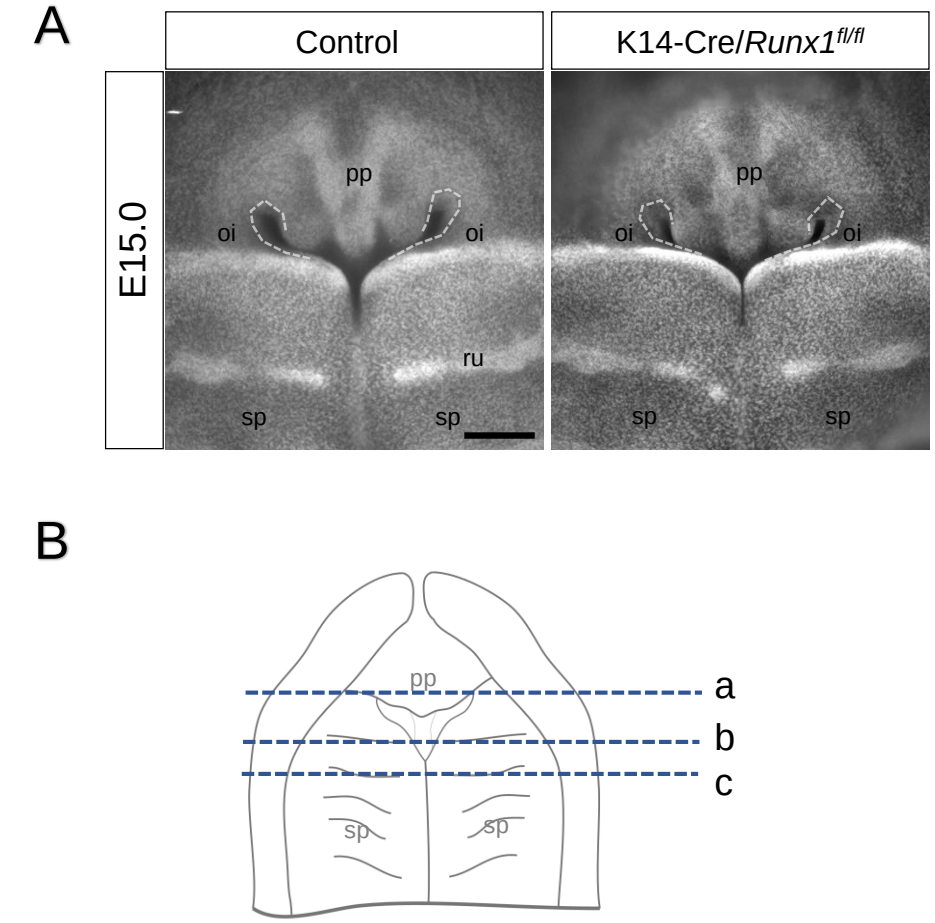
A
Control
K14-Cre/Runx1fl/fl
E15.0
pp
oi
oi
ru
sp
sp
B
pp
a
b
c
sp
sp
C
Control
K14-Cre/Runx1fl/fl
K14-Cre/Cbfbfl/fl
BrdU
a
b
E15.0
pp
sp

Figure 3

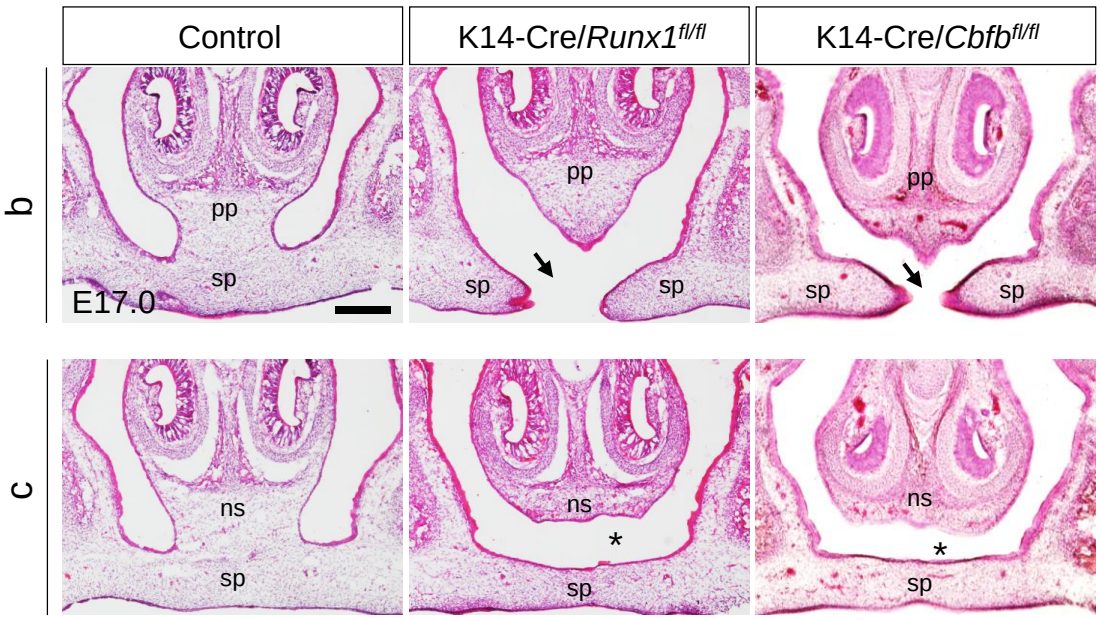
A
Control
K14-Cre/Runx1fl/fl
K14-Cre/Cbfbfl/fl
b
c
pp
sp
E17.0
ns
*

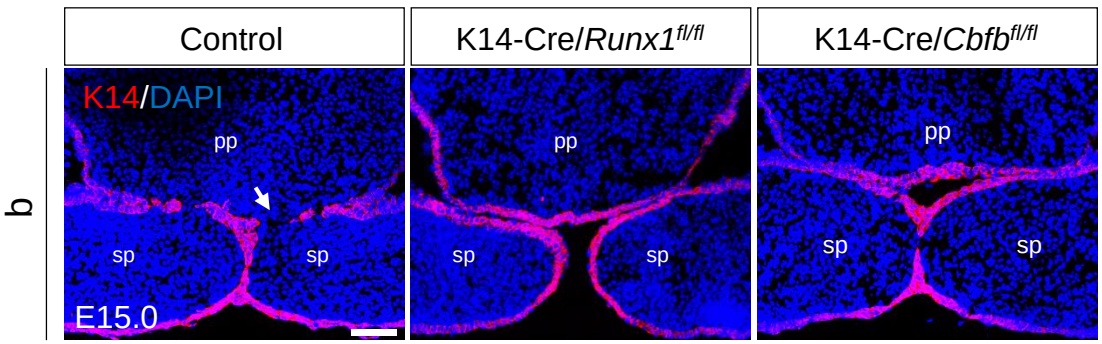
B
Control
K14-Cre/Runx1fl/fl
K14-Cre/Cbfbfl/fl
b
K14/DAPI
pp
sp
E15.0

Figure 4

A

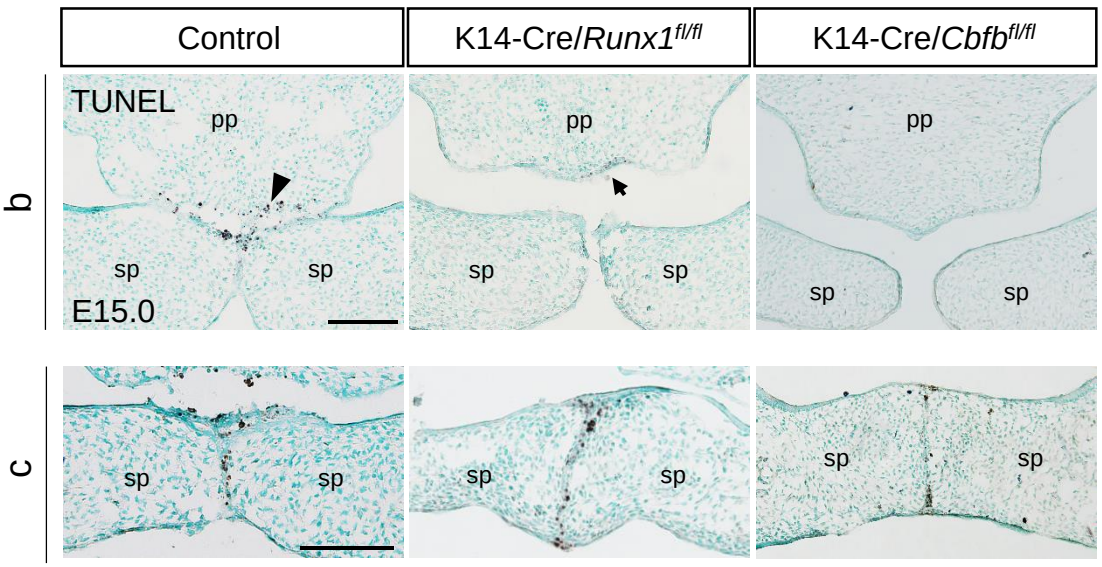
Control
K14-Cre/Runx1fl/fl
K14-Cre/Cbfbfl/fl
b
c
TUNEL
pp
sp
E15.0

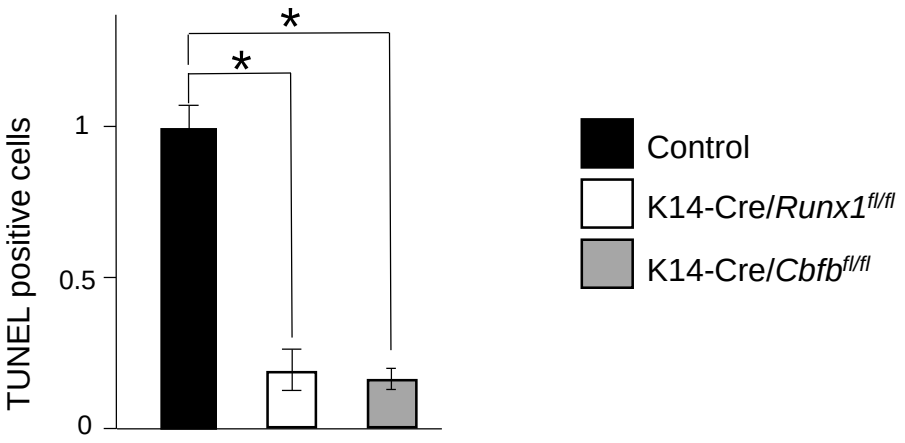
TUNEL positive cells
1
0.5
0
*
*
Control
K14-Cre/Runx1fl/fl
K14-Cre/Cbfbfl/fl

Figure 5

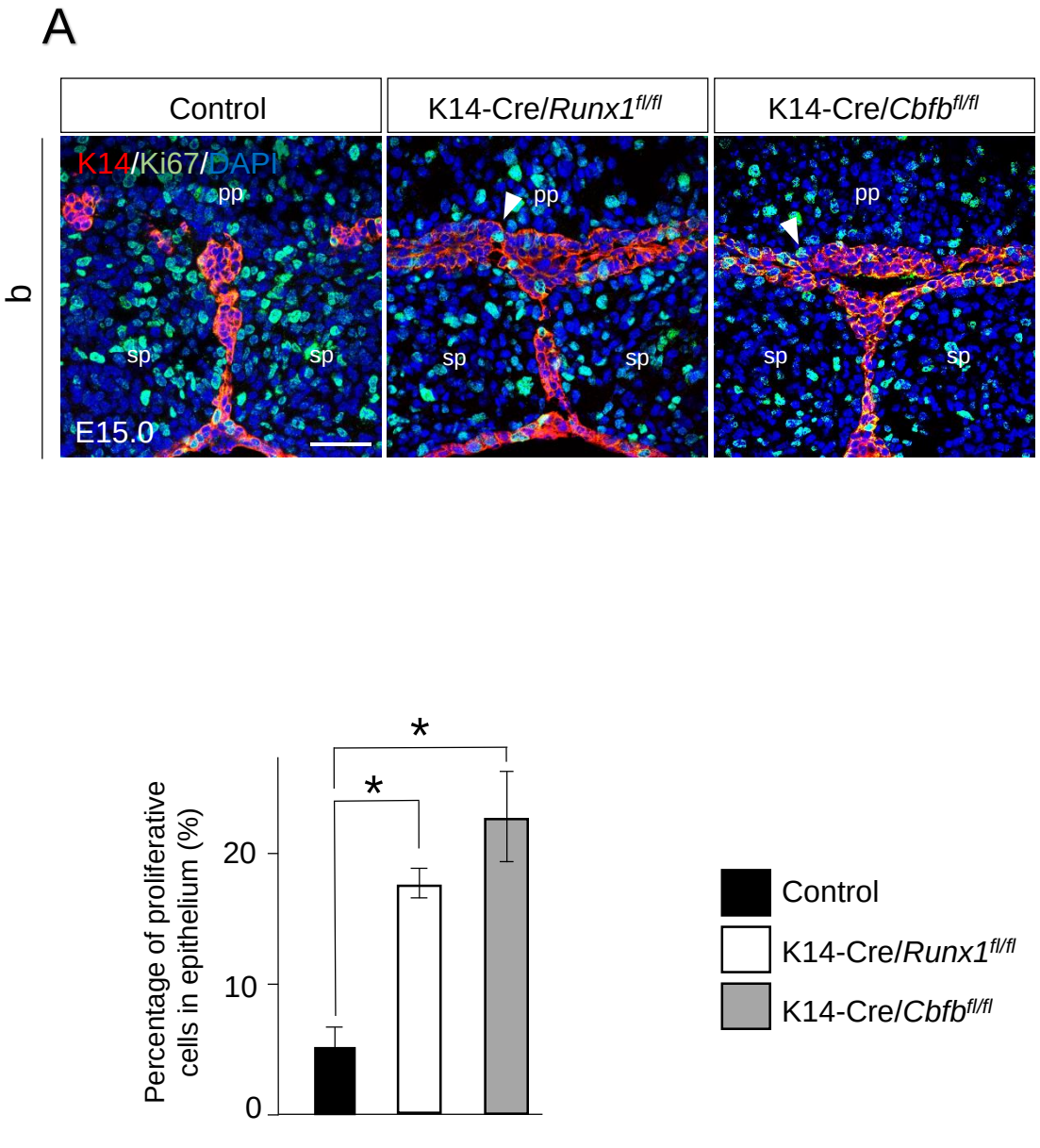
A
Control
K14-Cre/Runx1fl/fl
K14-Cre/Cbfbfl/fl
b
K14/Ki67/DAPI
pp
sp
E15.0
Percentage of proliferative cells in epithelium (%)
0
10
20
*
*
Control
K14-Cre/Runx1fl/fl
K14-Cre/Cbfbfl/fl

Figure 6

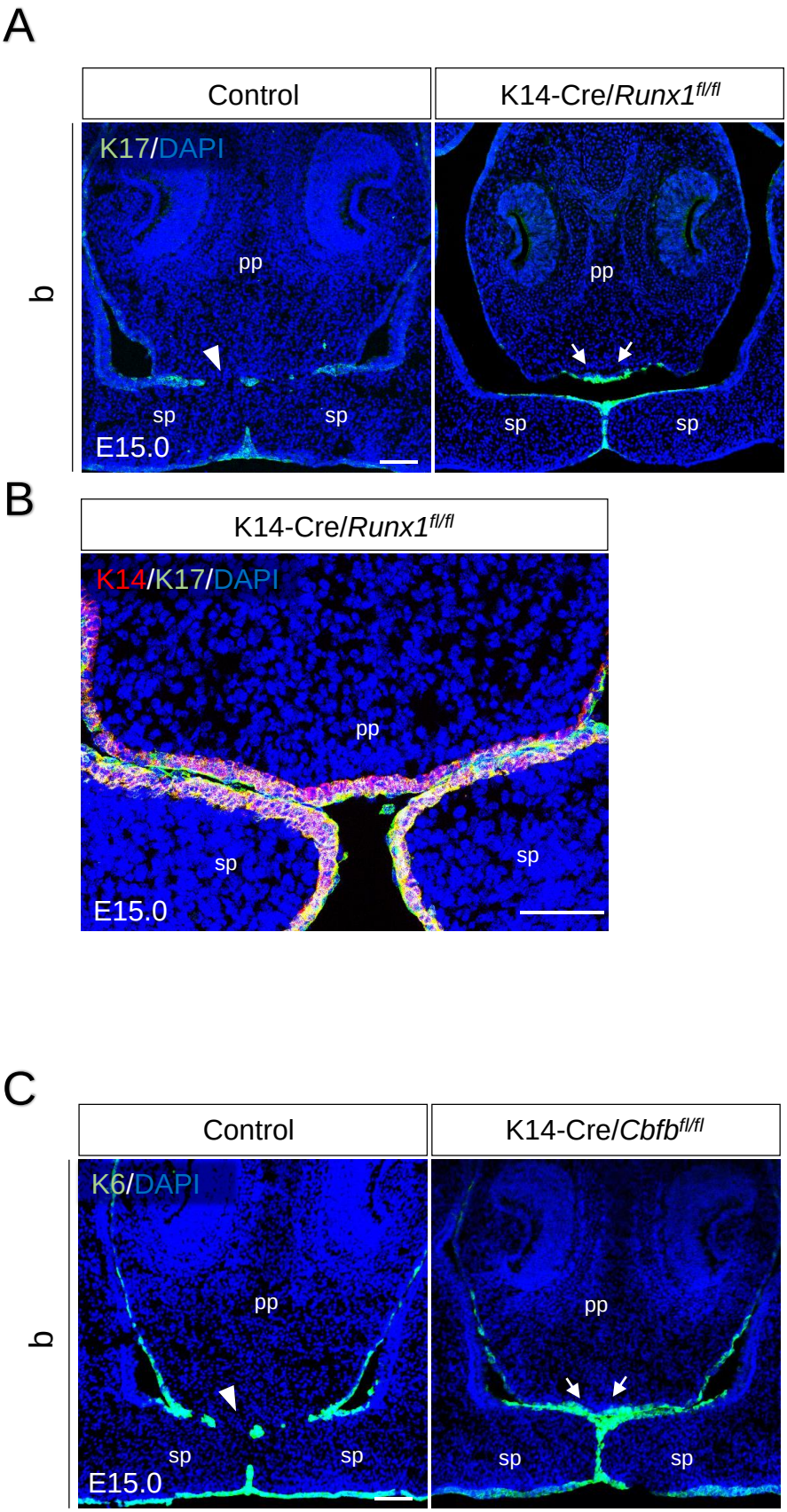
A
Control
K14-Cre/Runx1fl/fl
K17/DAPI
pp
sp
sp
E15.0
b
B
K14-Cre/Runx1fl/fl
K14/K17/DAPI
pp
sp
sp
E15.0
C
Control
K14-Cre/Cbfbfl/fl
K6/DAPI
pp
sp
sp
E15.0
b

Figure 7

A

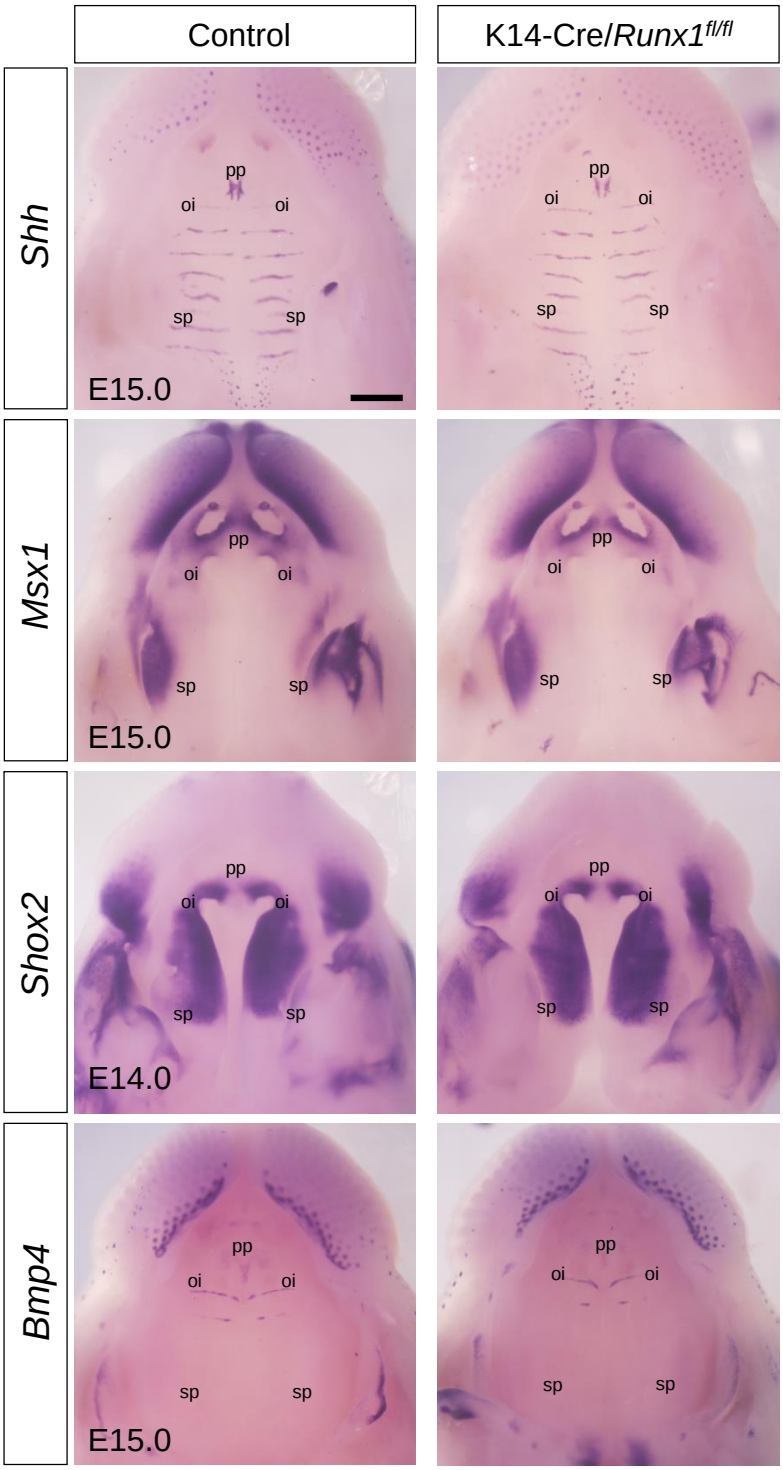
Control
K14-Cre/Runx1fl/fl
Shh
Msx1
Shox2
Bmp4
pp
oi
oi
sp
sp
E15.0
E14.0

Figure 8

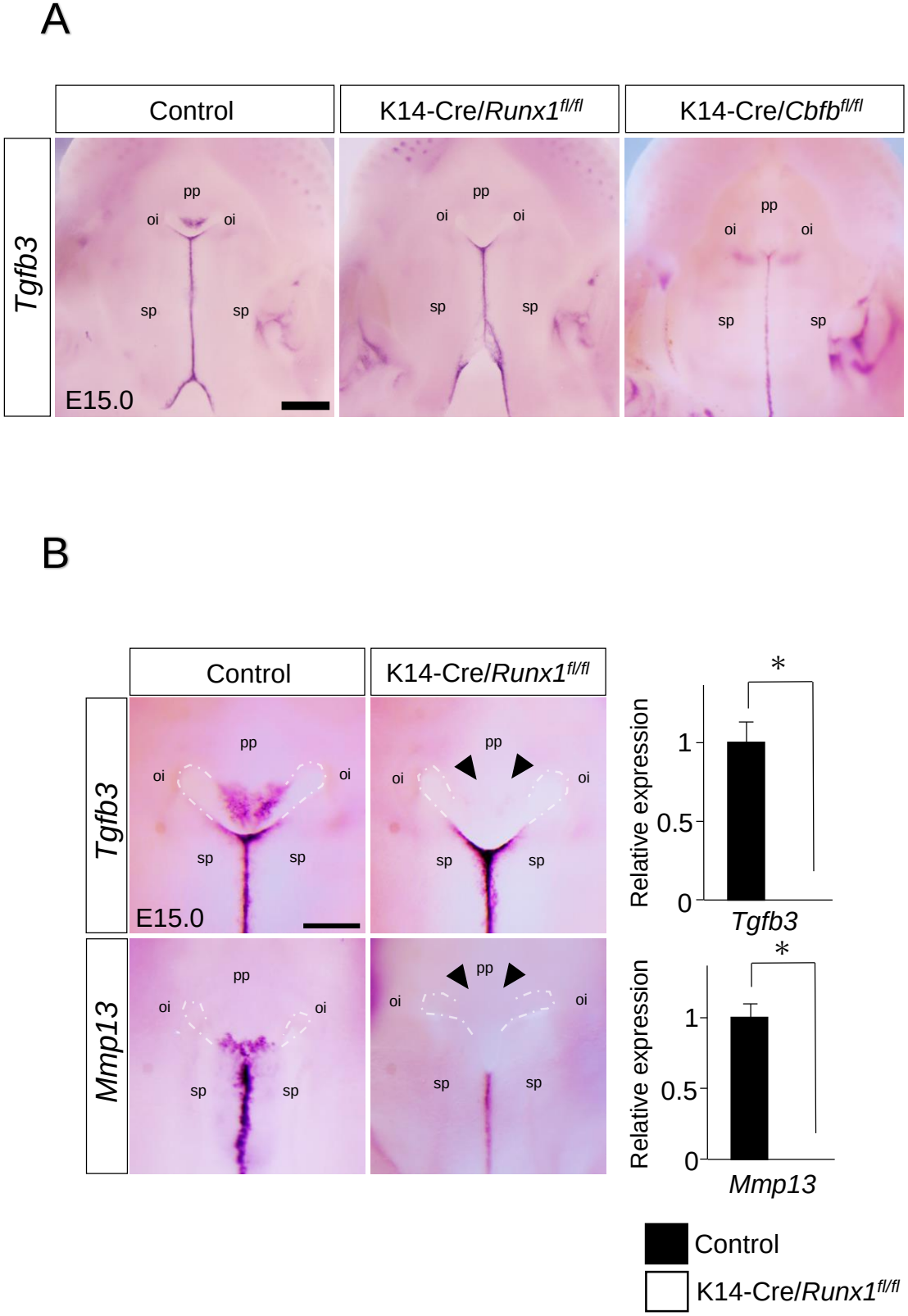
A
Control
K14-Cre/Runx1fl/fl
K14-Cre/Cbfbfl/fl
Tgfb3
pp
oi
oi
sp
sp
E15.0
B
Control
K14-Cre/Runx1fl/fl
Tgfb3
Mmp13
Relative expression
1
0.5
0
*
Tgfb3
Mmp13
Control
K14-Cre/Runx1fl/fl

Figure 9

A

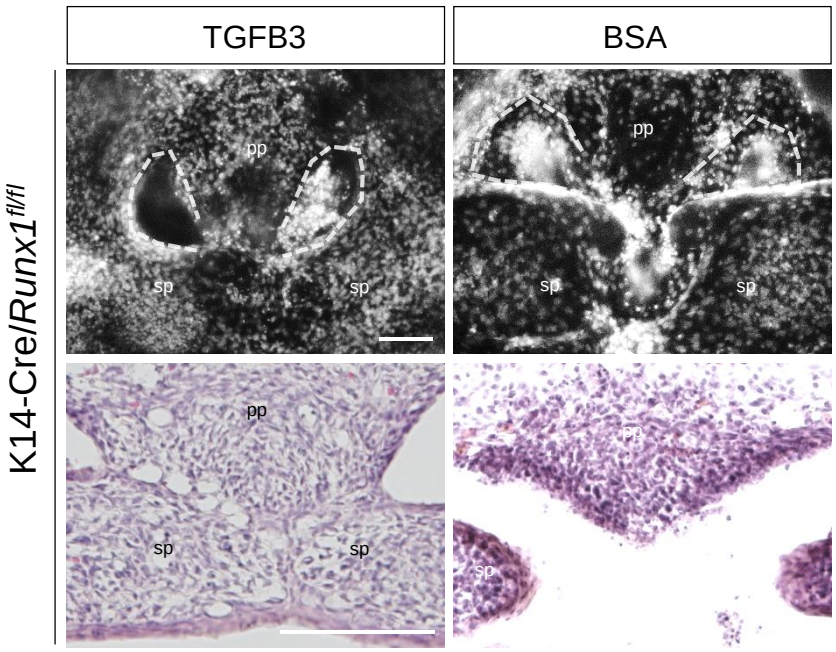

B

Anterior palate fusion assessment

BSA	0%	(0/6)
TGFB3	75%	(6/8)

C

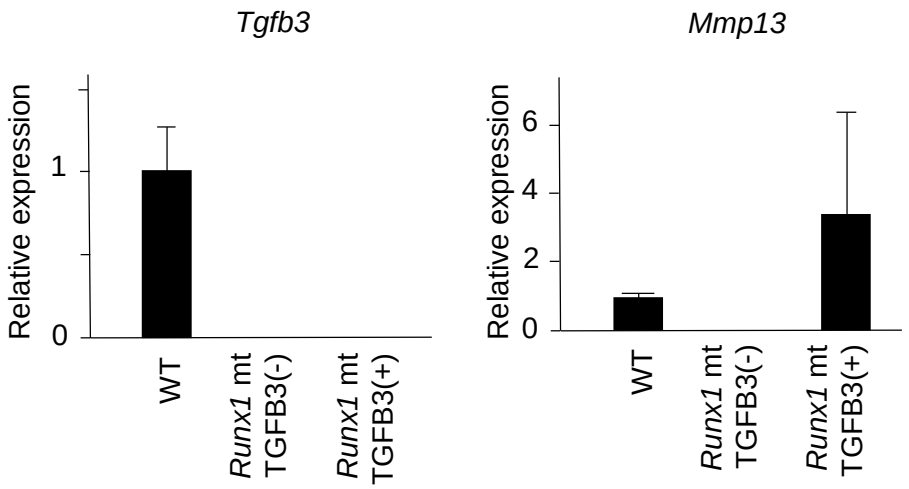

Figure 10

A

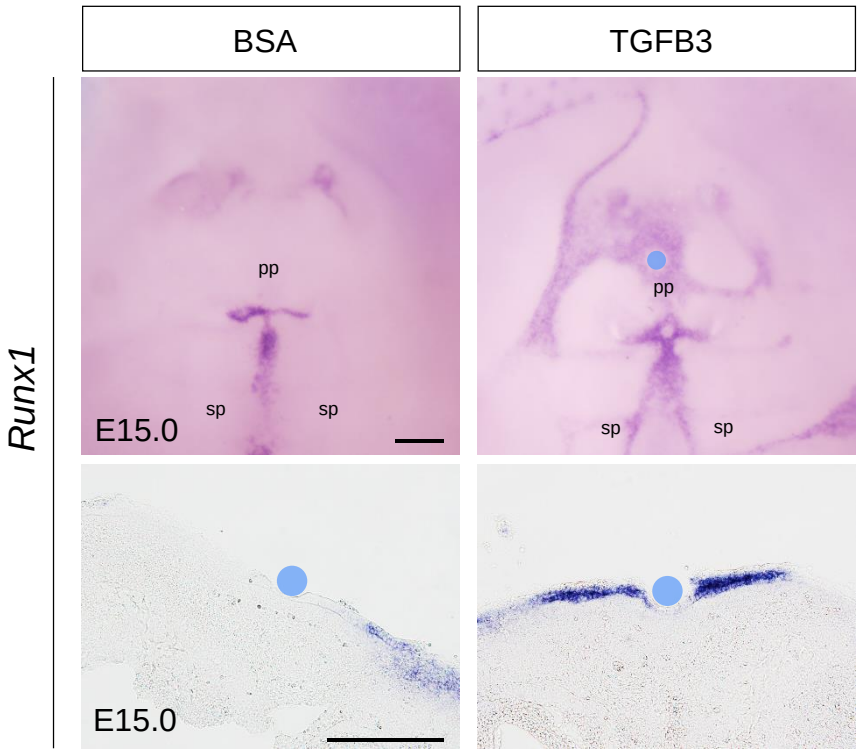

Figure 11

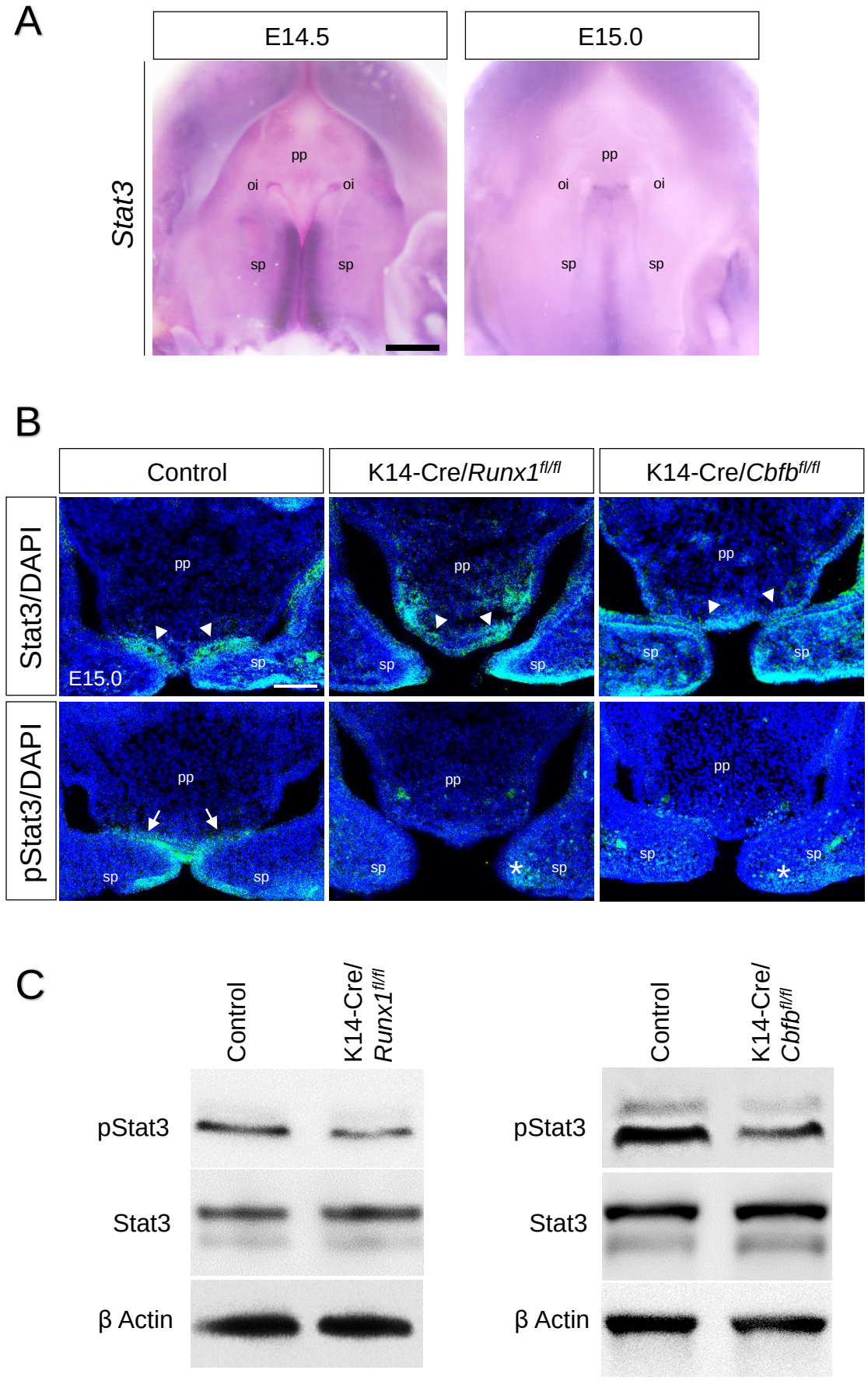
A
E14.5
E15.0
Stat3
pp
oi
oi
sp
sp
B
Control
K14-Cre/Runx1fl/fl
K14-Cre/Cbfbfl/fl
Stat3/DAPI
pStat3/DAPI
E15.0
C
Control
K14-Cre/Runx1fl/fl
Control
K14-Cre/Cbfbfl/fl
pStat3
Stat3
β Actin

Figure 12

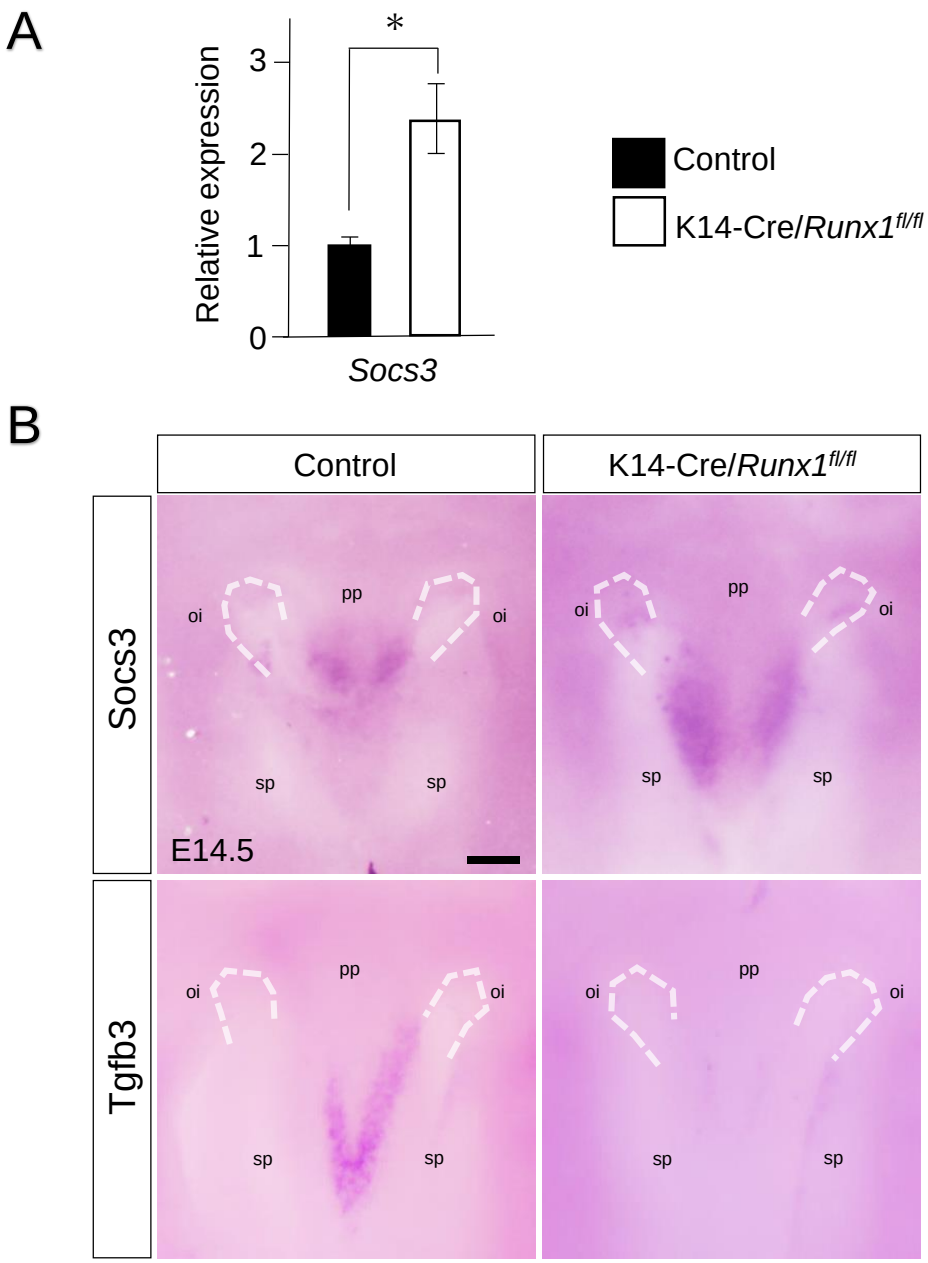
A
*
Relative expression
3
2
1
0
Socs3
Control
K14-Cre/Runx1fl/fl
B
Control
K14-Cre/Runx1fl/fl
Socs3
Tgfb3
pp
oi
oi
sp
sp
E14.5

Figure 13

A

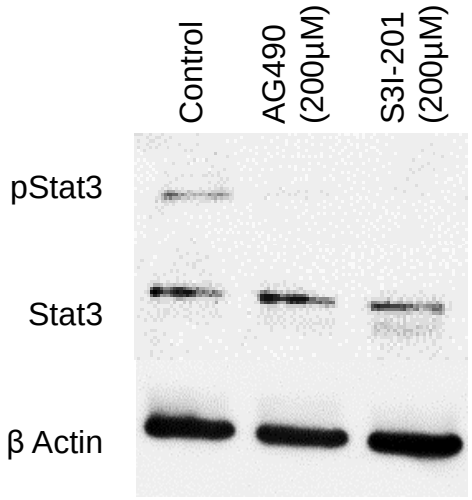

B

Frequency of Anterior Cleft		
	Possibility	
Control	0%	(0/6)
AG490 (200μM)	100%	(8/8)
AG490 (400μM)	100%	(11/11)
S3I-201(200μM)	90%	(9/10)
S3I-201 (400μM)	100%	(10/10)

C

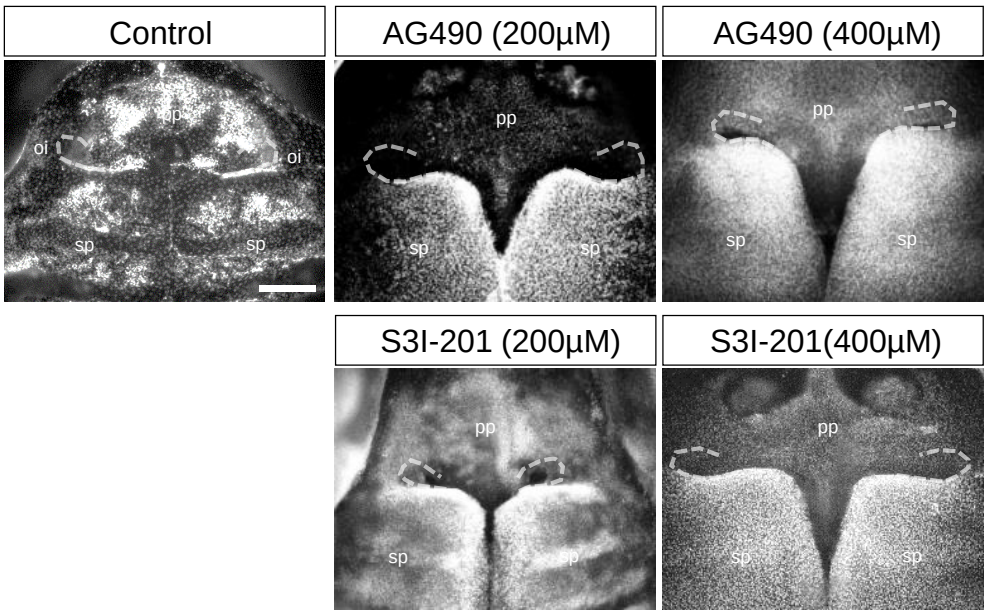

Figure 14

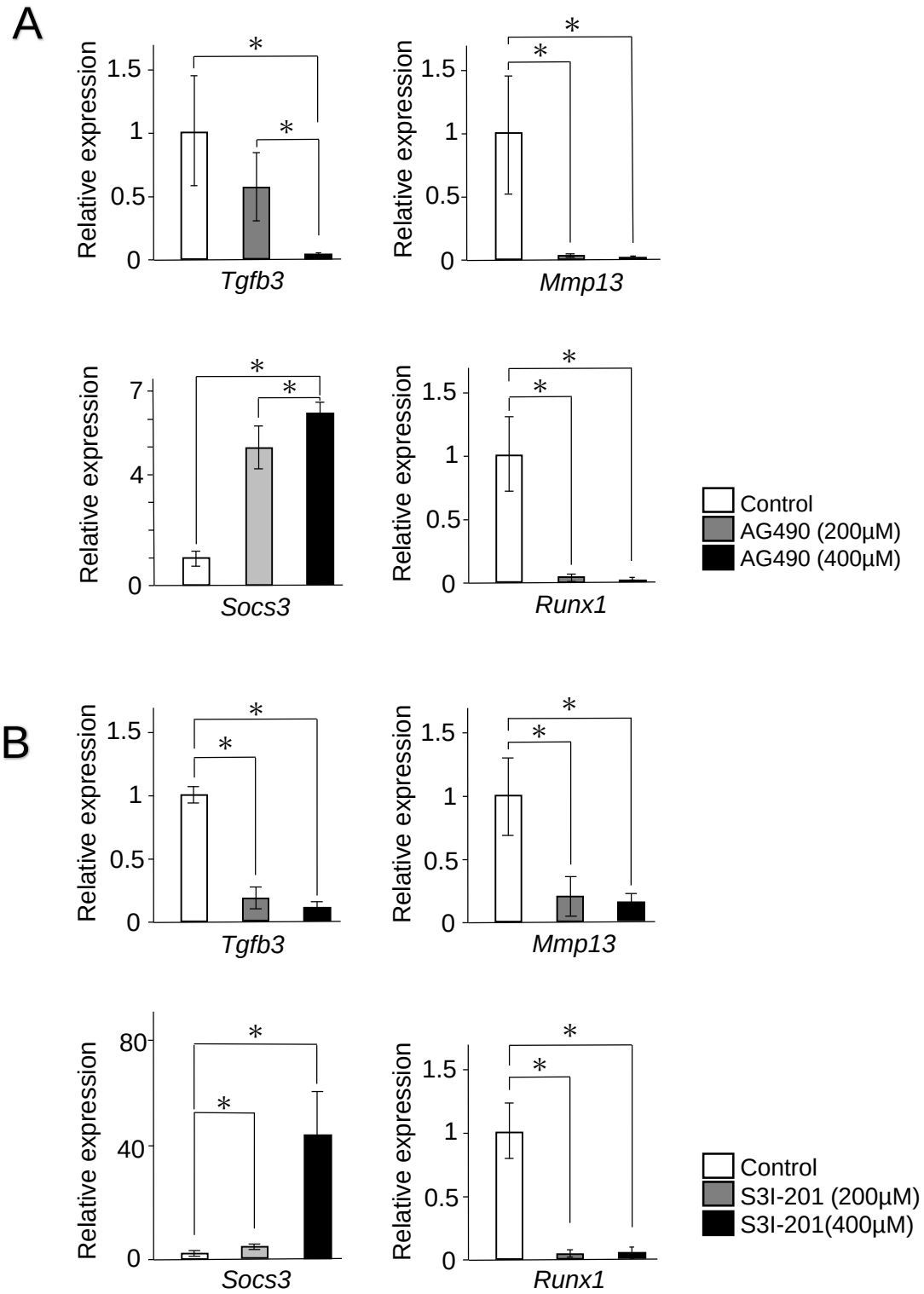
A
Relative expression
1.5
1
0.5
0
Tgfb3
Mmp13
7
4
Socs3
Runx1
Control
AG490 (200μM)
AG490 (400μM)
B
80
40
S3I-201 (200μM)
S3I-201(400μM)

Figure 15

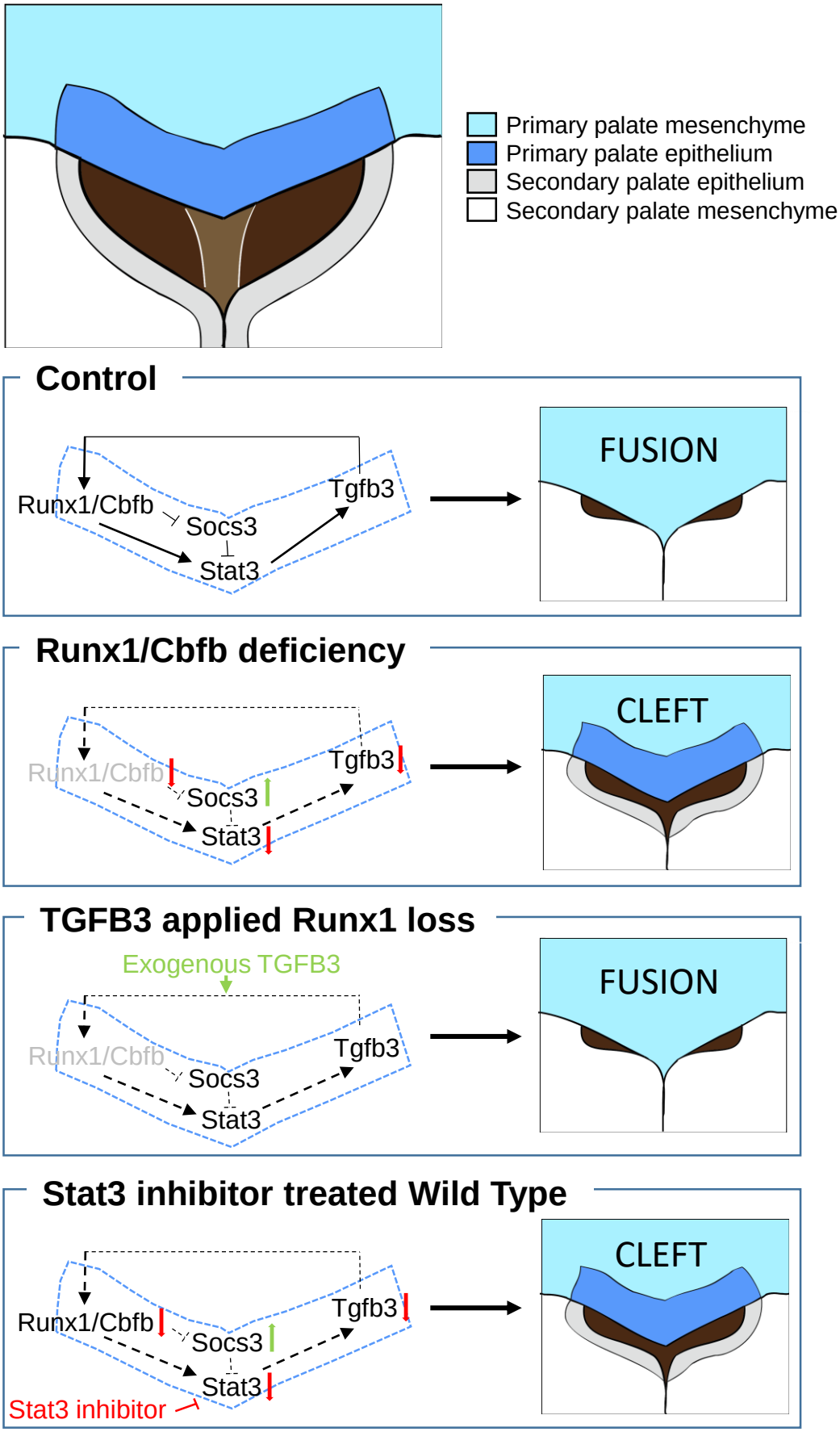
Primary palate mesenchyme
Primary palate epithelium
Secondary palate epithelium
Secondary palate mesenchyme
Control
Runx1/Cbfb
Socs3
Stat3
Tgfb3
FUSION
Runx1/Cbfb deficiency
Runx1/Cbfb
Socs3
Stat3
Tgfb3
CLEFT
TGFB3 applied Runx1 loss
Exogenous TGFB3
Runx1/Cbfb
Socs3
Stat3
Tgfb3
FUSION
Stat3 inhibitor treated Wild Type
Runx1/Cbfb
Socs3
Stat3
Tgfb3
Stat3 inhibitor
CLEFT

Figure 16

Quantitive PCR Primer Sequences	
GENE	Primer Sequence
Gapdh	F: 5' - AACTTTGGCATTGTGGAAGG - 3'
	R: 5‘ - ACACATTGGGGGTAGGAACA - 3'
Runx1	F: 5' - CAGCATGGTGGAGGTACTAG - 3'
	R: 5‘ - AGGTCGTTGAATCTCGCTAC - 3'
Tgfb3	F: 5' - CTGGACACCAATTACTGCTTC - 3'
	R: 5‘ - TGGGTTCAGGGTGTTGTATAG - 3'
Mmp13	F: 5' - AAGATGTGGAGTGCCTGATG - 3'
	R: 5‘ - AAGGCCTTCTCCACTTCAGA - 3'

Probe PCR Primer Sequences	
GENE	Primer Sequence
Runx1	F: CATTTAGGTGACACTATAGAGCATGGTGGAGGTACTAGCTG
	R: TAATACGACTCACTATAGGGGCGCCGTAGTATAGATGGTAGG
Tgfb3	F: CATTTAGGTGACACTATAGGGAGCCCCTGACCATCTT
	R: TAATACGACTCACTATAGGGAGGCTCCCCGGATACTTG
Mmp13	F: CATTTAGGTGACACTATAGCCAAAACACCAGAGAAGTGTGA
	R: TAATACGACTCACTATAGGGCTTCATAGCACGCAAGAATCAG
Stat3	F: CATTTAGGTGACACTATAGGAGGCCCTCCCAACATCT
	R: TAATACGACTCACTATAGGGTTCATTCCAAAGGGCCAA

Figure 17